Reversible hydrogen storage in multilayer graphane: lattice dynamics, compressibility, and heat capacity studies

Volodymyr A. Yartys [a], Vladimir E. Antonov [b], Boris M. Bulychev [c], Vadim S. Efimchenko [b], Valery I. Kulakov [b], Mikhail A. Kuzovnikov [d], Ross T. Howie [d], Hannah A. Shuttleworth [d], Mylaine Holin [d], Rebecca Rae [d], Matthew B. Stone [e], Boris P. Tarasov [f], Radion I. Usmanov [g,b], Alexander I. Kolesnikov [e,*]

[a] *Institute for Energy Technology, P.O. Box 40, Kjeller NO-2027, Norway*

[b] *Institute of Solid State Physics RAS, 142432 Chernogolovka, Moscow District, Russia*

[c] *Moscow State University, Leninskiye Gory, 119991Moscow, Russia*

[d] *Centre for Science at Extreme Conditions and School of Physics and Astronomy, University of Edinburgh, Edinburgh EH9 3FD, United Kingdom*

[e] *Neutron Scattering Division, Oak Ridge National Laboratory, Oak Ridge, TN 37831, USA*

[f] *Institute of Problems of Chemical Physics RAS, 142432 Chernogolovka, Moscow District, Russia*

[g] *National Research University Higher School of Economics, 20 Myasnitskaya ul., 101000 Moscow, Russia*

Keywords:
Multilayer graphane
Hydrogen storage
High-pressure
Equation of state
Inelastic neutron scattering
Phonons
Heat capacity

---

* Corresponding author.

E-mail address: kolesnikovai@ornl.gov (A.I. Kolesnikov).

Graphical Abstract

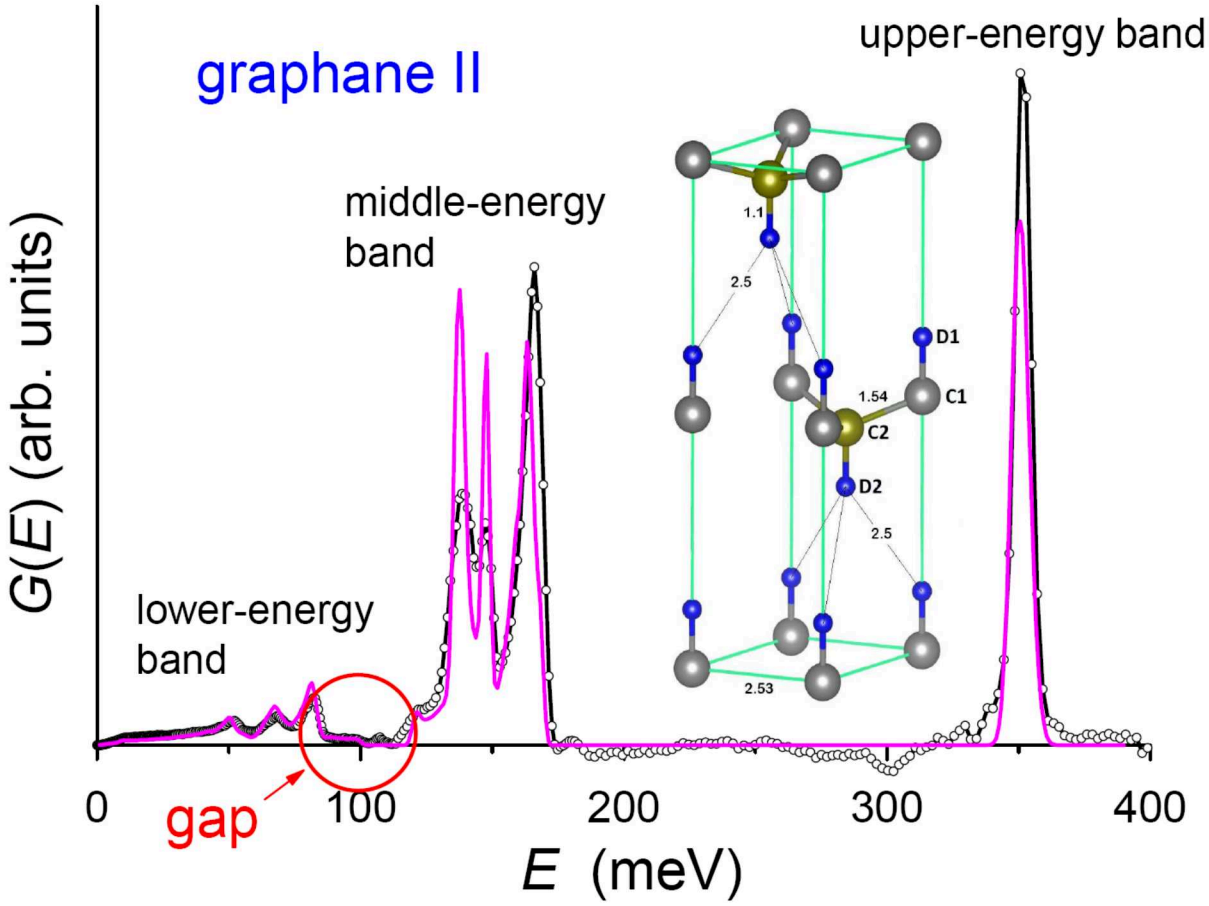

Experimental (circles) and calculated (line) spectra of the generalized phonon density of states $G(E)$ of multilayer graphane.

Scientific highlights

- Single-phase samples of graphite hydride CH and deuteride CD were synthesized
- The lattice dynamics of both samples was studied by inelastic neutron scattering
- A chair form of graphane was formed as evidenced by a gap in the INS spectra
- Compressibility, thermal expansion, heat capacity of graphite hydride were measured
- Once formed, graphite hydride is stable at H_2 pressures up to 53 GPa at $T \leq 1500$ K

ABSTRACT

Multilayer graphane (hydride of graphite) is a crystalline hydrocarbon of composition CH, which can be synthesized from graphite and molecular hydrogen at pressures above 2 GPa [V.E. Antonov et al., Carbon 100 (2016) 465]. Using X-ray diffraction, this compound was tentatively identified as the "graphane II" phase of 3D-graphane predicted by *ab initio* calculations [X.-D. Wen et al., PNAS 108 (2011) 6833] and consisting of layers of 2D-graphane in the "chair" conformation. When heated in a vacuum, the compound does not form any intermediate hydrocarbons and reversibly decomposes back into graphite and hydrogen at 770–920 K. In the present work, almost single-phase samples of graphite hydride and deuteride were synthesized at 7.4 GPa and 870 K. Their investigation by inelastic neutron scattering supplemented by *ab initio* calculations gave spectra $g(E)$ of the phonon density of states with a gap of about 15 meV at approx. 100 meV, which is a unique identifier for the chair form of graphane. The equation of state $V(P)$ of the hydride was studied at room temperature and hydrogen pressures up to 53 GPa by synchrotron X-ray diffraction in a diamond anvil cell. The graphane II phase did not react with the surrounding hydrogen and did not undergo any phase transformations upon the compression and after heating to 1500 K at 53 GPa. The high thermal and pressure stability of this exotic phase makes it an important part of the C-H system. The obtained $g(E)$ spectra of graphite hydride and deuteride were used to calculate temperature dependences of their heat capacity. Measurements of the heat capacity at temperatures 120–673 K confirmed the good accuracy of these calculations.

1. Introduction

Graphane is a free-standing sheet of graphene coated on both sides with hydrogen atoms covalently bonded to the carbon atoms. The thermodynamic stability of graphane was predicted by *ab initio* calculations [1,2], and later such an unusual two-dimensional hydrocarbon was synthesized by the reaction of graphene with atomic hydrogen [3]. This gave rise to many theoretical studies of the structure and properties of a single-layer, double-layer and multilayer (bulk) graphanes. One of the most detailed and comprehensive *ab initio* studies [4] predicted mechanical stability of several different phases of multilayer graphane with CH stoichiometry at high pressures and $T = 0$ K. According to [4], the $P\bar{3}m1$ "graphane I" and $P6_3mc$ "graphane II" phases consisting of graphane layers in the "chair" conformation stacked in the –AAAA- and -ABAB- sequences, respectively, are stable at pressures of 0–10 GPa and have almost equal enthalpies. The pressure interval of 10–240 GPa is the region of stability for a denser *Cmca* "graphane III" phase composed of layers of graphane in the "boat" conformation. A later first-principles investigation [5] of phase equilibria in the C-H system at pressures up to 400 GPa and temperatures of 0, 500, 1000, and 2000 K showed that the graphane I phase has no range of stability if van der Waals corrections are taken into account. The graphane III phase should be stable at pressures of 18–46 GPa and $T = 0$ K and unstable at any pressure at temperatures of 500 K and above.

Multilayer graphane was synthesized in 2016 [6] by the reaction of graphite powder with molecular hydrogen at pressures 2–7.5 GPa and temperatures 720–970 K. The surface of the powder particles was preliminarily activated by ball milling under fairly mild conditions (30 min at 250 rpm in Ar) that did not significantly affect their crystallinity. The chemical composition of the resulting multilayer graphane was close to CH. The samples were thermally stable under ambient conditions and decomposed into graphite and hydrogen at 770–920 K when heated in vacuum at a rate of 20 K/min. That is, the hydrogenation of graphite is a reversible process.

The crystal structure of the hydrogenated samples was studied by X-ray diffraction at room temperature. A semi-quantitative comparison of the obtained powder diffraction patterns with those calculated for the predicted [4] phases of multilayer graphane showed that the graphane II structure provides the best fit. The lattice parameters of its hexagonal $P6_3mc$ unit cell were refined to $a = 2.53(1)$ Å and $c = 9.54(1)$ Å, which exceeded the corresponding unit cell parameters of graphite by 2.4(2) % and 42.0(3) %, respectively. The value of $a = 2.53$ Å and the distance $c/2 = 4.77$ Å between the graphane layers agree with those predicted for the multilayer graphane in the chair conformation (see, e.g., [7,8]). The positions of the H and D atoms in the unit cell could not be reliably determined by X-ray diffraction, and these atoms were placed at a distance of $0.12c \approx$

1.1 Å in the *c*-direction from the nearest C atom, since the length of 1.1 Å is typical of a singular C–H bond in any hydrocarbon.

The graphane II structure of graphite deuteride proposed in Ref. [6] is schematically shown in Fig. 1. The graphane layers are weakly bound by van der Waals forces. Each hydrogen atom in these layers is attached to an individual carbon atom from alternate sides of the layer plane, and this carbon atom is displaced (buckled) out of the hexagonal plane toward its bonded hydrogen atom. According to Ref. [6], the displacement equals to $0.05c/2 \approx 0.25$ Å and results in the increase in the minimum distance between the neighboring C atoms in the buckled layer to $d_{C–C} \approx 1.54$ Å, which is noticeably larger than $d_{C–C} = a/\sqrt{3} \approx 1.46$ Å in a flat carbon layer with the same lattice parameter $a = 2.53$ Å. The distance $d_{C–C} \approx 1.54$ Å agrees with predictions of most *ab initio* calculations (see, e.g., [7,4]).

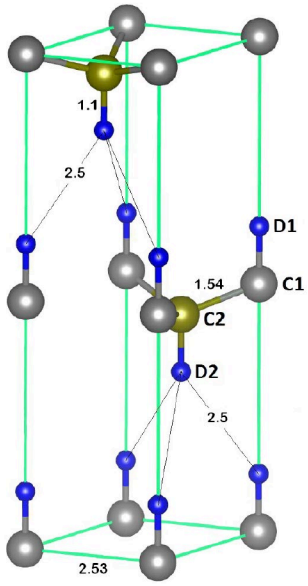

Fig. 1. The $P6_3mc$ structure of a CD crystal of graphane II phase [6]. Large spheres represent C atoms; small spheres stand for D atoms. The atoms labeled C1 and D1 occupy 2*a* positions; those labeled C2 and D2 are on the 2*b* positions. The numerical values indicate interatomic distances in Angstroms. A description of the structure is given in the file "CD-II_exp.cel" in Supplementary Material (its URL is indicated in appendix A).

The formation of graphane-like 3D-crystals with a size of 2–4 nm was also observed in amorphous benzene partially crystallized at 8–10 GPa and 930–1000 K by Kondrin et al. [9]. The complex structure of the nanocrystals was modeled in a *Pbca* orthorhombic unit cell ($a = 9.63$; $b = 9.02$; $c = 17.2$ Å) with 16 carbon and 16 hydrogen atoms in general positions. The distance between the graphane layers varied from 4.75 to 4.9 Å and decreased with increasing temperature and pressure of the sample synthesis. The layers contained fragments of graphane in the chair conformation. Most likely, the authors of Ref. [9] observed an intermediate stage of crystallization of benzene into the graphane II phase, while the complete transformation was hindered due to its sluggish kinetics.

We are not aware of other successful attempts to synthesize multilayer graphane. At the same time, studies of the domain of stability, composition, crystal structure, thermodynamic and physical properties of hydrocarbons formed at high pressures and temperatures are of significant

fundamental importance as evidenced, in particular, by the abiotic origin of deposits of methane and other hydrocarbons formed in the upper mantle of the Earth [10,11]. The experiments [6,9] have shown that multilayer graphanes can be stable over a wide temperature and pressure range up to 1000 K and 10 GPa and therefore this unusual type of hydrocarbons deserves a careful investigation.

Diffraction methods alone are insufficient to unambiguously determine the crystal structure of graphanes, since graphite itself is replete with various defects, and its crystal structure is additionally damaged during the ball-milling and subsequent hydrogenation causing an approximately 50% volume increase. In fact, the X-ray diffraction study [6] only allowed the authors to choose between the two structures, graphane I and graphane II, which were previously predicted as the most stable phases of multilayer graphane at pressures below 10 GPa and consisted of graphane layers in the chair conformation [4].

Meanwhile, the *ab initio* calculations [4] also predicted that the graphane I and graphane II phases strikingly differ from other phases of the 3D-graphane by the presence of a gap of approximately 15 meV between the lower- and middle-energy phonon bands, which is characteristic of the phonon spectrum of single-layer graphane in the chair conformation (see, e.g., [12–14]). This provided the opportunity to verify the interpretation of the X-ray diffraction data [6] by studying the lattice dynamics of the synthesized 3D-graphane. Hydrogenated and deuterated samples of graphite were studied in Ref. [6] by infrared spectroscopy, but instead of the light absorption by the regular crystal structure in the bulk of the material, the measured spectra showed light scattering by the CH, CH_2 and CH_3 defect groups covering the surface of graphane particles. The high shielding efficiency of these groups was attributed to the small penetration depth of the light.

In the present work, the vibrational spectra of hydride and deuteride of graphite were studied at $T = 5$ K by inelastic neutron scattering (INS), which gave spectra averaged over the entire sample volume. The measurements were supplemented by DFT calculations of the crystal structure, electronic structure and lattice dynamics of the graphane I, II, and III phases of multilayer graphane. The results of our calculations were all in good agreement with those in the literature (e.g., in Refs. [7,8,4]). Nevertheless, these new calculations were necessary because most literature results were not presented in numeric form and could not be used for accurate estimates. The calculations helped us, in particular, to convert the measured INS spectra into the spectra $g(E)$ of the phonon density of states. The "experimental" $g(E)$ spectra thus obtained showed a clearly distinguished gap of about 15 meV between the lower- and middle-energy bands, which unambiguously confirmed that the synthesized hydride and deuteride were built from graphane layers in the chair conformation. The "experimental" and theoretical $g(E)$ densities of phonon

states were used to calculate the temperature dependences of the heat capacity $C_V(T)$ for graphite hydride and deuteride at temperatures up to 1000 K. To facilitate further experimental and theoretical studies, these and some other results of the paper are presented in numerical format in Supplementary Material.

We also studied the equation of state $V(P)$ of graphite hydride by Synchrotron X-ray diffraction in a diamond anvil cell at room temperature and pressures of 0.3–53 GPa using molecular hydrogen as a pressure transmitting medium. At room temperature, the structural parameters of the sample showed no anomalies or phase transitions upon increasing the pressure and, also, after heating to 1500±500 K in an H_2 atmosphere at the maximum pressure of 53 GPa. This indicates a very high thermal and pressure stability of the graphane II phase (for comparison: one of the most stable hydrocarbons CH_4, when mixed with molecular hydrogen, forms new compounds $CH_4(H_2)_2$, $(CH_4)_2H_2$ [15], and $(CH_4)_3(H_2)_{25}$ [16] at pressures below 11 GPa). Fitting the experimental $V(P)$ dependence for graphite hydride with the Birch-Murnaghan equation of state [17,18] gave the bulk modulus B_0 = 22.5 GPa and the specific volume V_0 = 13.19(3) Å^3/atom C under ambient conditions. The latter value is in excellent agreement with the experimental V(1 atm) = 13.22(1) Å^3/atom C from Ref. [6].

Another portion of the hydride sample was studied by X-ray diffraction at ambient pressure and temperatures from 297 to 573 K. Using the semi-empirical Grüneisen law claiming that the coefficient α of thermal expansion is approximately proportional to the heat capacity, we fitted the experimental $V(T)$ dependence and extrapolated the obtained $V_{fit}(T)$ and $\alpha_{fit}(T)$ dependences down to T = 0 K and up to T = 1000 K. Using B_0 = 22.5 GPa and another Grüneisen's semi-empirical dependence $\beta = 1/B_0 \propto V^{8.4}$ established for the isothermal compressibility β, we obtained the $\beta(T)$ dependence, calculated the difference $\Delta C_{PV} = C_P - C_V = \alpha^2 VT/\beta$, and converted the dependence $C_V(T)$ resulting from $g(E)$ to the dependence $C_P(T)$ of heat capacity at constant pressure. Due to the high compressibility of the hydride, the term $\Delta C_{PV}(T)$ turned out to be small compared to other contributions to the heat capacity. The $C_V(T)$ dependence for deuteride of graphite was converted to $C_P(T)$ by adding $\Delta C_{PV}(T)$ determined for the graphite hydride.

Finally, the heat capacity of the synthesized hydride and deuteride of graphite was measured with a differential scanning calorimeter at temperatures of 120–673 K and coincided with the calculated $C_P(T)$ dependences well within the experimental error. This confirmed the self-consistency and sufficient accuracy of the measurements and approximations made in the present study.

2. Experimental details and data treatment

2.1. Pre-treatment of graphite

The starting material was high-purity graphite containing 4×10^{-5} wt.% Fe; 1×10^{-4} wt.% Si; 2×10^{-5} wt.% Ca, and less than 1×10^{-5} wt.% of other impurities (electrode quality). Previous experiments have shown [6] that graphite flakes and plates of bulk graphite do not react with molecular hydrogen at pressures up to 9 GPa and temperatures up to 720 K. In Ref. [6], the chemical activity of graphite increased after ball milling under mild conditions (30 min at 250 rpm) in a protective Ar atmosphere. The milled graphite reacted with hydrogen at high pressures and elevated temperatures, but the yield of the multilayer graphane was limited to 60–70% in most experiments. One of the reasons for the low yield of the reaction could be the poisoning of the particles of the milled graphite by impurities of active gases present in the Ar gas filling the ball mill. In this paper, we used graphite milled 30 min at 250 rpm in a planetary ball mill Fritsch Pulverisette 6 filled with hydrogen at a pressure of 1 MPa. Graphite is known to absorb hydrogen up to the atomic ratio H/C ≈ 0.95 in the course of amorphization under intense ball milling (80 h at 400 rpm) in molecular hydrogen compressed to 1 MPa [19]. The graphite milled in our work had a low hydrogen content $H/C < 1.5\cdot10^{-3}$. To prevent deactivation in air, this starting material was stored in an argon glove box. The high-pressure hydrogenation of the material prepared in this way ensured the conversion of graphite to graphane with a yield of 88–97%.

2.2. High-pressure synthesis of hydride and deuteride of graphite

A 126 mg sample of graphite hydride was collected from several batches prepared by exposing ≈30 mg portions of the milled graphite to a hydrogen pressure of 7.4(3) GPa at a temperature of 870(15) K for 2 hours. Hydrogen was produced inside the high-pressure cell using thermal decomposition of an internal hydrogen source, amminoborane NH_3BH_3, incased into a tightly plugged silver capsule together with the graphite powder and separated from it by a thin layer of Pd (the method is described in more detail elsewhere [20]). The amount of gaseous H_2 released from NH_3BH_3 was 3 times greater than the amount of hydrogen absorbed by the sample. The pressure of 7.4 GPa was the maximum pressure attainable with the Toroid-type [21] high-pressure chamber used in this paper, while the temperature of 870 K was chosen to get the maximum hydride yield (the yield is lower at lower temperatures due to the kinetic reasons, while at temperatures above 1000 K, the hydride transforms into methane and/or other light hydrocarbons [6]). The hydrogen content of a small portion of each batch of the hydrogenated graphite was examined by hot extraction of the hydrogen into a pre-evacuated calibrated volume in the regime of heating the sample to 930 K at a rate of 20 K/min (see [6] for details). The collected sample

with the total mass of 126 mg had an average atomic ratio of H/C = 0.94(3) and, therefore, consisted of 94 mol.% of hydride with C/H = 1 and 6 mol.% of unreacted graphite. The sample showed no hydrogen loss or reaction with air after being stored under ambient conditions for 6 months.

A 146 mg sample of deuterated graphite was prepared in the same manner using aluminum trideuteride as an internal deuterium source. Unfortunately, the trideuteride was contaminated with protium, so the graphite deuteride was also contaminated with protium and had the composition $CD_{0.91}H_{0.09}$ according to our INS investigation. Hot extraction gave a mean value of (D+H)/C = 0.95(3) for this sample, so it contained 5 mol.% of unreacted graphite.

2.3. Measurements by inelastic neutron scattering

The INS spectra of the samples of the hydrogenated and deuterated graphite were measured with SEQUOIA, the fine-resolution Fermi chopper spectrometer at the Spallation Neutron Source at Oak Ridge National Laboratory [22]. The INS data were collected at 5 K with four incident neutron energies E_i = 420, 220, 120, and 55 meV selected by the high-flux Fermi chopper rotating, respectively, at 600, 360, 300, and 240 Hz and providing a good energy resolution ($\Delta E/E_i$) of about 1.5% to 3%. Each powder sample was encased in a flat aluminum container 50×50×0.1 mm^3 in size, which was placed perpendicular to the incoming neutron beam. The data were recorded over a wide range of scattering angles from –30° to +60° in the horizontal plane and ±18° in the vertical direction.

Prior to further treatment, the collected data were transformed from the time-of-flight and instrument coordinates to the dynamical structure factor $S(Q,E)$, where Q and E were the neutron momentum and energy transfers. The background spectra for the empty containers were measured under the same conditions and subtracted from the original data. Contour plots of $S(Q,E)$ for the samples of graphite hydride and deuteride measured at T=5 K and each selected incident neutron energy E_i = 55, 120, 220, and 420 meV are shown in Supplementary Material (Figs. S1 and S2, respectively). These spectra were then transformed into the almost spectrometer-independent, generalized phonon density of states $G(E)$ and merged together. To reduce the undesired contribution to $G(E)$ from multiple neutron scattering events at small scattering angles, the data recorded in the range from –15° to +15° for E_i = 420, 220, and 120 meV and in the range from –25° to +25° for E_i = 55 meV were excluded from the calculations. A one-phonon spectrum $G^{1ph}(E)$ for the hydride was obtained from $G(E)$ by subtracting the multiphonon contribution calculated in an isotropic harmonic approximation using an iterative technique [23,24].

Unlike H atoms, D and C atoms scatter neutrons predominantly coherently, so to obtain the vibrational density of states of graphite deuteride it was necessary to average neutron scattering data over a wide range of neutron momentum transfers. The quality of the averaging can be assessed by the ratio R of the volume of reciprocal space covered in the INS experiment to the volume of the Brillouin zone of the crystal [25]. In our INS investigation of graphite deuteride, the condition of averaging was fulfilled in the whole range 2–400 meV of energy transfers, as the spectrometer provided $R \approx 80$ for $E_i = 55$ meV and $R > 300$ for higher $E_i = 120$, 220, and 420 meV.

2.4. Modeling the lattice dynamics of graphite hydride and deuteride

The vibrational properties of graphane I, II, and III phases of hydride and deuteride of graphite were also modeled with a density-functional theory implemented in the CASTEP code [26]. The calculations were performed using the LDA functional [27] as parametrized by Perdew and Zunger [28]. The LDA functional was chosen because it satisfactorily reproduces interplanar bonding in graphite, whereas the more common GGA functional does not (see [29] for discussion). Norm-conserving pseudopotentials with a plane-wave cutoff energy of 680 eV were used. The dynamical matrices were calculated with the density functional perturbation theory [30]. To produce full $g_{calc}(E)$ and partial $G_{calc}(E)$ phonon densities of states, the Brillouin-zone integration was performed according to the Monkhorst-Pack scheme [31] with a 23 × 23 × 5 sampling for graphane II, a 9 × 9 × 4 sampling for graphane I, a 8 × 8 × 5 sampling for graphane III, and a 5 × 5 × 2 sampling for the compound $C_{16}D_{14}H_2$, which was used to model the lattice dynamics of the experimental graphane II sample with the composition $CD_{0.91}H_{0.09}$.

Figure 2 shows the calculated phonon dispersion relations for the graphane II phases of graphite hydride (a) and deuteride (b) and for the graphane I phase of graphite hydride (c). The dependences for the graphane I phase well agree with those calculated in Ref. [4]; the dependences for the graphane II phases have not been published previously. As one can see from Fig. 2, the phonon spectra of both the graphane I and II phases consist of three bands, which we will further call the lower-, middle-, and upper-energy bands. The lower band of the graphane I phase with two CH groups in the unit cell is formed by acoustic vibrations (3 phonon states) and the two higher bands represent optical vibrations (9 phonon states).

The lower band of the graphane II phase with four CH groups in the unit cell also stems from acoustic vibrations, but its unit cell is doubled compared to graphane I, so the Brillouin zone is folded in half. For example, the phonon modes from the A and Γ points in graphane I will both appear in the Γ point in graphane II, etc. This looks as there were low-lying optical modes in graphane II (compare Figs. 2a and 2c). The number of phonon states in graphane II is doubled

compared to graphane I, so there are 6 states in the lower-energy band, 14 states in the middle-energy band, and 4 states in the upper-energy band (the total number of phonon modes is 3×4×2 = 24). The folding of the Brillouin zone does not physically affect the phonon density of states as long as the interaction between the graphane layers is weak.

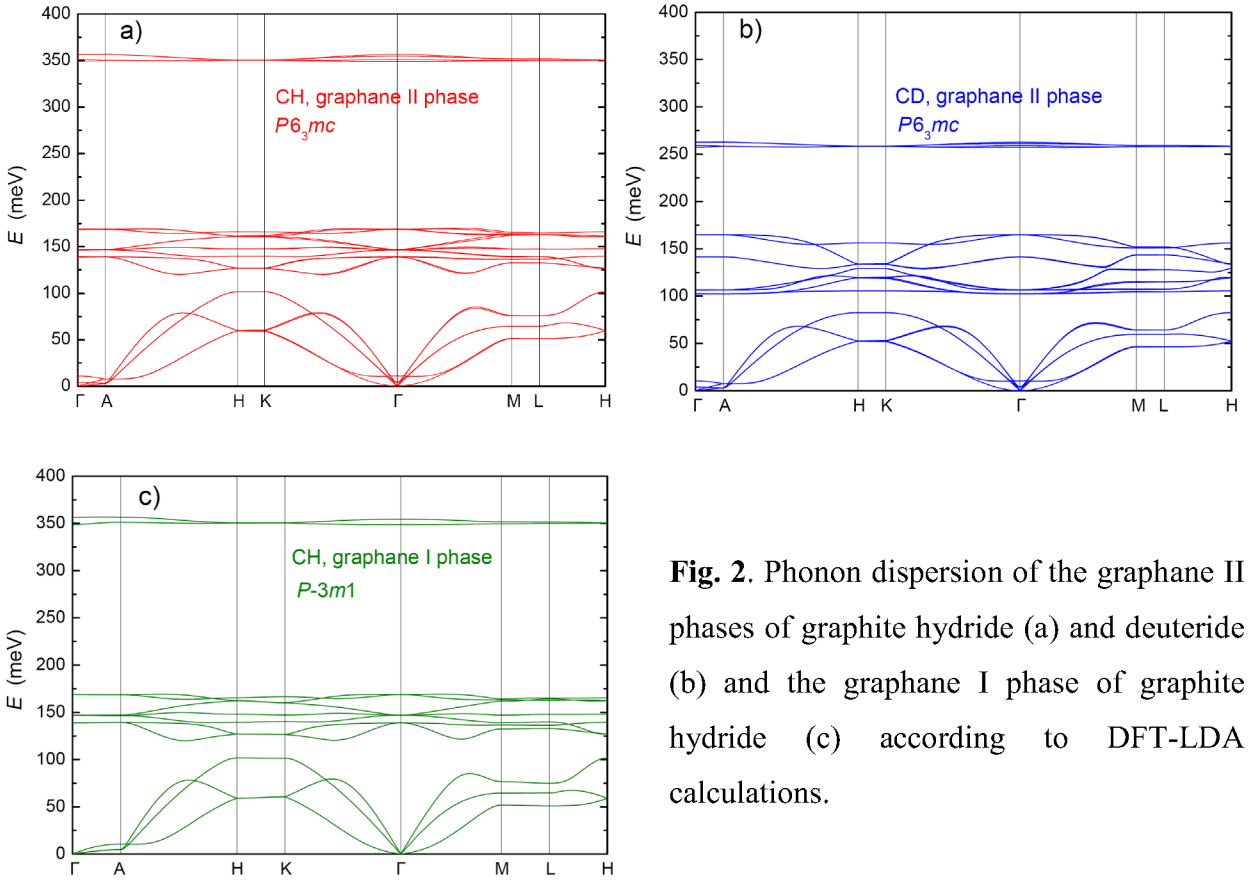

Fig. 2. Phonon dispersion of the graphane II phases of graphite hydride (a) and deuteride (b) and the graphane I phase of graphite hydride (c) according to DFT-LDA calculations.

The $G_{calc}(E)$ spectrum calculated for the graphane II phase of the hydride agreed with its experimental one-phonon $G^{1ph}(E)$. Based on the calculated phonon density of states $g_{calc}(E)$, the $G^{1ph}(E)$ spectrum was transformed into the "experimental" $g(E)$ by renormalizing the integrated area under the $G^{1ph}(E)$ curve to the proper number of vibrational modes. To model the lattice dynamics of the deuteride $CD_{0.91}H_{0.09}$ contaminated with protium, we considered a stoichiometric compound $C_{16}D_{14}H_2$ (or $CD_{0.875}H_{0.125}$, which is the same) derived from graphane II. The structural parameters of this compound resulted from our DFT calculations are presented in the file "C16D14H2_calc.cel" in Supplementary Material. The calculations gave $g_{calc}(E)$ for the $CD_{0.875}H_{0.125}$ compound and partial $G_i(E)$ for the C, D, and H atoms. These $G_i(E)$ were used to construct $G_{calc}(E)$ for the $CD_{0.91}H_{0.09}$ sample, and this $G_{calc}(E)$ spectrum represented well the main features of the experimental $G(E)$.

A comparison of the experimental parameters for graphite hydride and deuteride with those calculated for the graphane II phase showed that the calculations underestimated the lattice

parameter a by 1.3% and parameter c by 5%. The phonon energies were underestimated by about 2% at $E < 200$ meV and by about 1% at $E > 200$ meV. In order to facilitate further use of the calculated phonon spectra, all $G_{calc}(E)$ and $g_{calc}(E)$ in this work were rescaled to eliminate this mismatch. The calculated structural parameters for the graphane I, II, and III phases are presented in the corresponding CEL files in Supplementary Material without any corrections.

2.5. X-ray diffraction studies of graphite hydride at high hydrogen pressures

To construct the $V(P)$ dependence for graphite hydride CH at pressures of 0–53 GPa at room temperature, we performed *in situ* X-ray powder diffraction measurements in diamond anvil cells (DACs). We used symmetric piston-cylinder DACs with wide apertures and diamonds of the Boehler-Almax design with flat culets 200 μm in diameter. Rhenium gasket was preindented at ~20 GPa and a hole with a diameter of ~120 μm was drilled in it using a custom-built IR laser drilling setup. The CH sample and a gold pressure standard [32] were placed into the DACs in air, and hydrogen gas (99.9995% purity, Linde) was loaded at a pressure of 0.2 GPa at room temperature with a gas-loading apparatus. Further compression was realized with a gas membrane. Hydrogen was always in excess, serving both as a reagent and as a pressure-transmitting medium. Angular-dispersive powder X-ray diffraction experiment was performed at the Extreme Conditions Beamline (ECB, P02.2) at PETRA-III, Hamburg, Germany [33], with an incident X-ray beam ($E = 42.6$ keV; $\lambda \approx 0.2914$ Å) focused to a ~2×2 μm^2 spot using Kirkpatrick-Baez mirrors. Diffraction images were recorded using a Perkin Elmer XRD1621 detector with a sample-to-detector distance (SDD) of ~400 mm calibrated with a CeO_2 standard. The calibration of SDD and wavelength, primary processing, azimuthal integration and background subtraction were done with the DIOPTAS v0.5.5 software [34]. Phase analysis was carried out using the POWDERCELL 2.4 program [35]. The lattice parameters a and c for the graphane II phase were determined from the positions of the 002 and 110 peaks.

2.6. X-ray diffraction studies of graphite hydride at elevated temperatures

Another small portion of the hydride sample was studied by X-ray diffraction in vacuum at temperatures of 297, 373, 473, and 573 K with a Rigaku SmartLab diffractometer using a multipurpose high-temperature attachment. The diffractometer was equipped with a 3kW copper tube, a primary beam monochromator of the Cu $K\alpha_1$ radiation, and a HyPix-3000 area detector. Prior to the measurements at each selected temperature, the diffractometer was self-aligned, so the zeroshift of the detector and displacement of the sample were temperature independent (this was

additionally verified by measuring the lattice parameter $a(T)$ of the platinum internal standard accurately determined previously [36]). The obtained diffraction patterns were analyzed using the Jana2006 program [37] with the Le Bail refinements using the 002 and 110 peaks only.

2.7. Calorimetric measurements

The heat capacity of the hydride and deuteride of graphite and, for comparison, of the initial ball-milled graphite was measured with a 5% accuracy at temperatures 120–673 K using a Perkin-Elmer DSC-7 differential scanning calorimeter. The measurements were carried out in the regime of heating at a rate of 20 K/min; the mass of each sample was about 13 mg. To ensure a good thermal contact with the sample holder, powder samples were enclosed into thin aluminum capsules and compacted under a pressure of 0.5 GPa into flat disks 6.6 mm in diameter and about 0.7 mm thick.

3. Results and discussion

3.1. Lattice dynamics of graphite hydride

The experimental $G(E)$ spectrum of graphite hydride is shown in Fig. 3. Based on Fig. 2a, one can distinguish the lower-energy band at $E < 100$ meV, the middle-energy band at $115 < E < 175$ meV, and the upper-energy band near 350 meV. The peaks at 286, 306 and 330 meV, as well as the hump-like feature between 200 and 260 meV, which are also observed in the experimental $G(E)$ spectrum, do not correspond to any predicted phonon modes. It was reasonable to attribute these features to multiphonon neutron scattering.

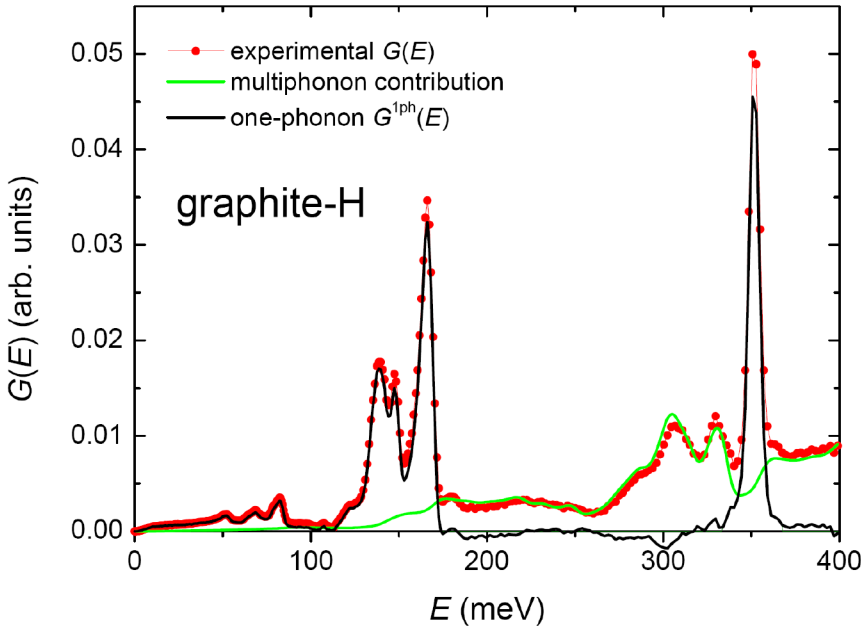

Fig. 3. Generalized phonon density of states $G(E)$ of graphite hydride measured at $T = 5$ K with the SEQUOIA neutron spectrometer at ORNL (solid red circles). The green curve shows the calculated contribution from multiphonon neutron scattering and the black curve represents the one-phonon $G^{1ph}(E)$ spectrum (black curve) obtained from $G(E)$ by subtracting the multiphonon contribution.

We calculated the multiphonon part of the $G(E)$ spectrum using a harmonic isotropic approximation and iterative technique [23,24] under the assumption that the one-phonon part of this spectrum is only located in the ranges 0–175 meV and 341–361 meV. The calculated multiphonon contribution is shown in Fig. 3 with a green curve and accurately describes the excess

scattering intensity at $E > 175$ meV. The difference between the experimental and multiphonon spectra can be assigned to the one-phonon spectrum $G^{1ph}(E)$ of the graphane phase.

As seen from Fig. 4a, the spectrum $G^{1ph}(E)$ thus obtained agrees with $G_{calc}(E)$ for the graphane II phase calculated in the LDA approximation and convoluted with the energy resolution function of the SEQUOIA spectrometer. In particular, the gap of the order of 15 meV between the lower- and middle-energy bands characteristic of graphanes in the chair conformation is clearly visible at energies near 100 meV. The contribution $G_i(E)$ of the atoms of type i to the total $G(E)$ of the compound is proportional to the ratio σ_i/m_i, where σ_i and m_i are the neutron scattering cross-sections and masses of the atoms. This ratio for the hydrogen atom is 177 times greater than for the carbon atom ($\sigma_H \approx 82$ barn and $m_H \approx 1.0$ amu, while $\sigma_C \approx 5.55$ barn and $m_C \approx 12.0$ amu) [38]. So, the $G(E)$ spectrum of graphane mainly represents the dynamics of hydrogen atoms.

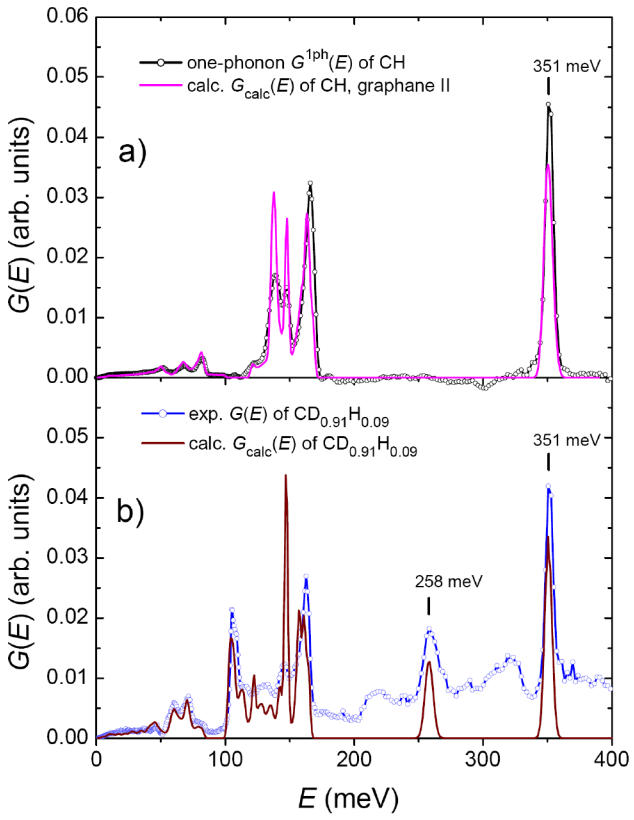

Fig. 4. (a) One-phonon spectrum $G^{1ph}(E)$ of graphite hydride taken from Fig. 3 (open black circles connected with a black curve) and calculated $G_{calc}(E)$ for the graphane II phase (solid magenta curve). (b) Generalized phonon density of states $G(E)$ of the graphite deuteride $CD_{0.91}H_{0.09}$ measured at $T = 5$ K with the SEQUOIA spectrometer at ORNL (open blue circles connected with a blue curve) and calculated $G_{calc}(E)$ for the graphane II phase of this compound (solid brown curve). The $G_{calc}(E)$ spectra were calculated in the LDA approximation and convoluted with the energy resolution function of the SEQUOIA spectrometer.

The intensity of the $G(E)$ spectrum is approximately proportional to the density $g(E)$ of phonon states of a hydride, and the latter can sometimes be accurately constructed by normalizing the integral intensity under the $G(E)$ curve to the number of phonon modes in the corresponding vibrational band. This has previously been demonstrated for α-AlH_3 [39] and α-MgH_2 [40], whose INS spectra were measured with good accuracy and energy resolution over the entire range of phonon frequencies. A specific feature of the graphane II phase is that the relative intensity of the

peak at ~125 meV in the middle-energy optical band of the calculated and experimental spectra $G(E)$ is about twice smaller than in the calculated $g_{calc}(E)$ spectrum (please compare Fig. 4(a) and Fig. 5a). This is because the peak is mostly related to the transverse optical C–C stretching modes, so the eigenvectors for the vibrations of H atoms corresponding to these modes are smaller than those for the other modes in the band. To get the "experimental" $g(E)$, we set the integral intensity of the 125 meV peak in $G(E)$ equal to 2 phonon states and renormalized the intensity of the other parts of the band to 12 states to obtain the required 14 states in total. The resulting experimental spectrum $g(E)$ is shown in Fig. 5a together with the calculated $g_{calc}(E)$.

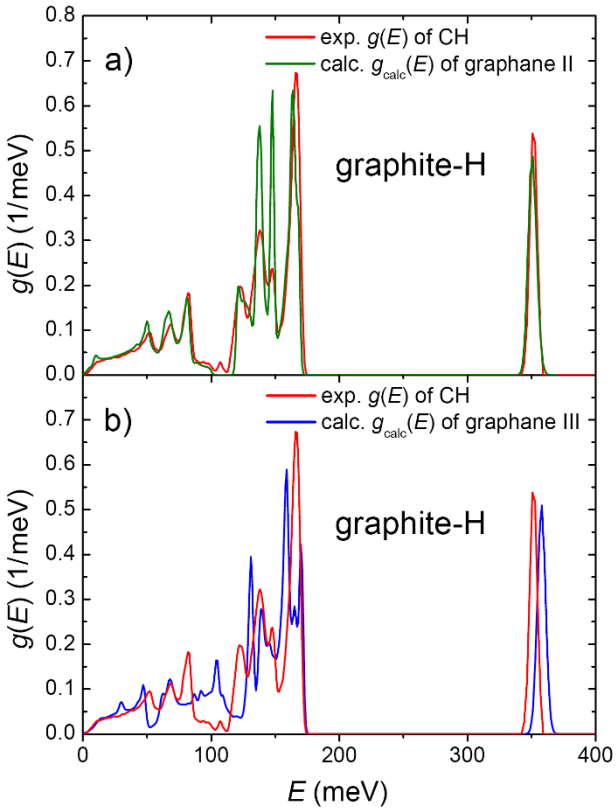

Fig. 5. Experimental phonon density of states $g(E)$ (solid red curve) and calculated phonon densities of states $g_{calc}(E)$ for the graphane II phase (olive curve) of graphite hydride (a) and for its graphane III phase (blue curve) (b). The $g_{calc}(E)$ spectra are calculated in the LDA approximation and convoluted with the energy resolution function of the SEQUOIA spectrometer.

The peak at 351 meV in Fig. 5a is formed by four modes of C–H stretching vibrations: two symmetrical and two antisymmetrical. As one can see, the full width at half maximum of the peak resulting from the INS measurements and from the DFT-LDA calculations is almost the same and equals to 7 meV, which is the energy resolution of the spectrometer. This indicates that the splitting of the stretching modes of graphite hydride and their dispersion are less than 7 meV in agreement with the *ab initio* calculations of the graphane II phase (see Fig. 2a).

Figure 5b compares the experimental $g(E)$ for the hydride of graphite (red curve) and calculated $g_{calc}(E)$ for the graphane III phase composed of layers of graphane in the boat conformation (blue curve). On the $g_{calc}(E)$ curve, a broad peak is observed with a maximum at 104

meV, right at the center of the interval of minimum experimental $g(E)$ values. Therefore, the synthesized multilayer graphane cannot have a crystal structure of the graphane III type.

At the same time, the INS method cannot distinguish the graphane II phase from the graphane I phase, while these phases should be almost equally stable at low pressures according to Ref. [4]. Indeed, our DFT calculations showed that the phonon spectra $g_{calc}(E)$ of the graphane I and II phases practically coincide (see Fig. 6a). Moreover, these spectra do not differ much from the phonon density of states calculated for the one-layer graphane in the chair conformation (see, e.g., [13] or [14]). The reason is that the vibrational spectrum of multilayer graphane is almost completely determined by the interactions between the atoms inside the graphane layers, since the layers are separated by a large distance of about 4.8 Å and weakly interact with each other. On the other hand, our INS investigation narrowed the range of possible modifications of the synthesized graphite hydride to the graphane I and graphane II phases, and the choice between them was unambiguously made previously in favor of the graphane II phase [6]. Figure S3 in Supplementary Material shows the X-ray data from Ref. [6], which illustrates the validity of this conclusion.

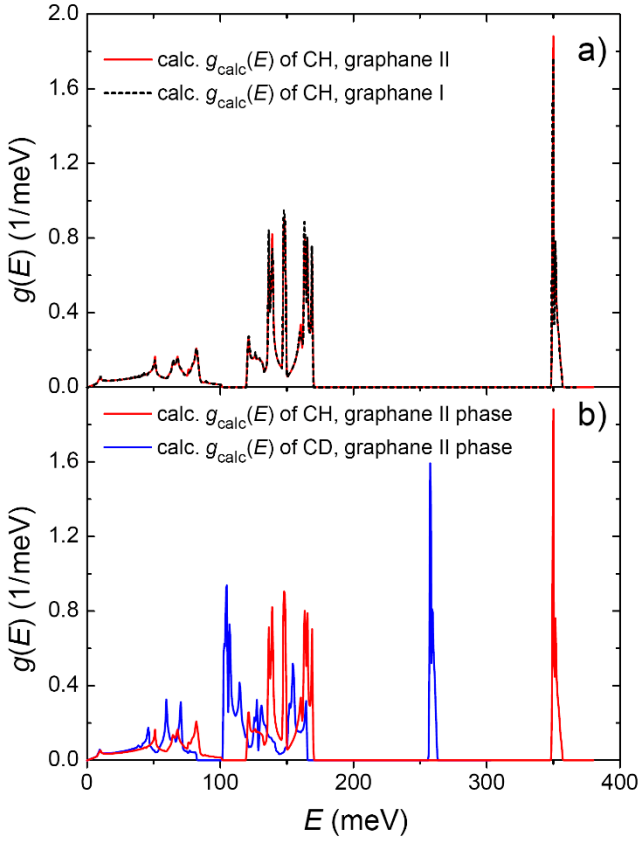

Fig. 6. Phonon density of states $g_{calc}(E)$ calculated in the LDA approximation: (a) for the phases graphane II (solid red curve) and graphane I (dashed black curve) of graphite hydride CH; (b) for the graphane II phases of graphite hydride CH (solid red curve) and graphite deuteride CD (solid blue curve). To facilitate comparison, the $g_{calc}(E)$ spectrum of each phase is normalized to 24 phonon states, as the spectrum of graphane II.

3.2. Lattice dynamics of graphite deuteride

As seen from Fig. 2, substituting deuterium for protium reduces all vibrational energies in the graphane II phase. Figure 6b compares $g_{calc}(E)$ for the graphane II phases of graphite hydride and graphite deuteride containing no H impurity. As one can see, the intensity distribution in the middle-energy band of the deuteride differs from that in the hydride, and the width of this band significantly increases. The gap between the lower- and middle-energy bands shifts below 100 meV, but its width remains almost unchanged and still equals to about 15 meV.

As we have already mentioned, the sample of graphite deuteride studied by INS was contaminated by protium. Our estimates of the effect of absorbed protium on the crystal structure and lattice dynamics of graphite deuteride are based on DFT calculations for a stoichiometric compound $C_{16}D_{14}H_2$ ($CD_{0.875}H_{0.125}$) with a $P6_3mc$ crystal structure of the graphane II type (see file "C16D14H2_calc.cel" in Supplementary Material). The calculated density of phonon states of this compound is presented in Fig. 7. Its most notable feature is the presence of a peak of stretching C–H vibrations occurring at exactly the same energy of 351 meV as in the pure hydride (please compare with Fig. 6). The position and shape of the C–D stretching peak and the lower-energy band remained virtually unchanged as well. Doping with protium somewhat changed the intensity distribution in the middle-energy band, but the energy span of this band remained practically the same. Since the protium concentration in the $CD_{0.875}H_{0.125}$ compound is higher than in the experimental $CD_{0.91}H_{0.09}$ sample, it can be expected that the phonon spectrum of the latter should differ from the spectrum of the pure CD phase in a similar way.

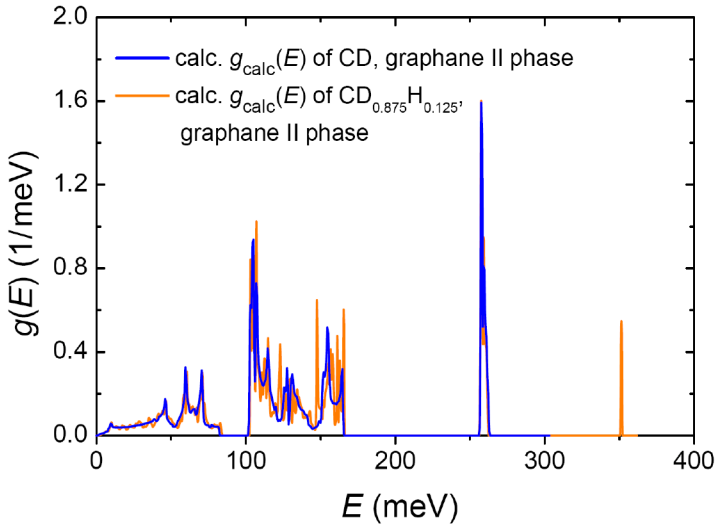

Fig. 7. Phonon density of states $g_{calc}(E)$ calculated in the LDA approximation for the graphane II phases of graphite deuteride CD (blue curve) and the $CD_{0.875}H_{0.125}$ compound (orange curve).

Using the calculated partial $G_i(E)$ for the C, D, and H atoms in the $CD_{0.875}H_{0.125}$ compound, we estimated $G_{calc}(E)$ for the already mentioned composition $CD_{0.91}H_{0.09}$ of the sample of graphite deuteride. The resulting total $G_{calc}(E)$ for the graphane II phase $CD_{0.91}H_{0.09}$ is shown by a solid brown line in Fig. 4b together with the experimental $G(E)$ determined by inelastic neutron scattering (open blue circles connected with a blue line). The peaks in $G_{calc}(E)$ at 258 and 351 meV are almost entirely due to the neutron scattering by the D and H atoms, respectively. The ratio D/H = 0.91/0.09 ≈ 10 for the experimental sample of graphite deuteride was estimated from the ratio of the integral intensities of the peaks of stretching H vibrations located at 351 meV in the INS spectra of the studied graphite hydride and deuteride (the peaks were fitted by Gaussians above the linearly sloped background).

The partial contributions of neutrons scattered by the C, D, and H atoms to the lower- and middle-energy bands of the total $G_{calc}(E)$ are shown by solid colored curves in Fig. 8. The contributions from 9 at. % H and 91 at. % D are comparable in magnitude, because σ_D = 7.64 barn [38] and m_D = 2 amu, which gives the ratio $(\sigma_H/m_H)/(\sigma_D/m_D) \approx 21$. Despite the complex nature of the calculated total $G_{calc}(E)$, it accurately reproduces the lower-energy part of the experimental $G(E)$ and reflects the main features of $G(E)$ in the middle-energy band, as one can see from Fig. 4b. Above the middle-energy band at E > 170 meV, a continuous and uneven spectrum of multiphonon neutron scattering overlaps with the one-phonon peaks of the C-D and C-H stretching vibrations located at 258 and 351 meV, respectively.

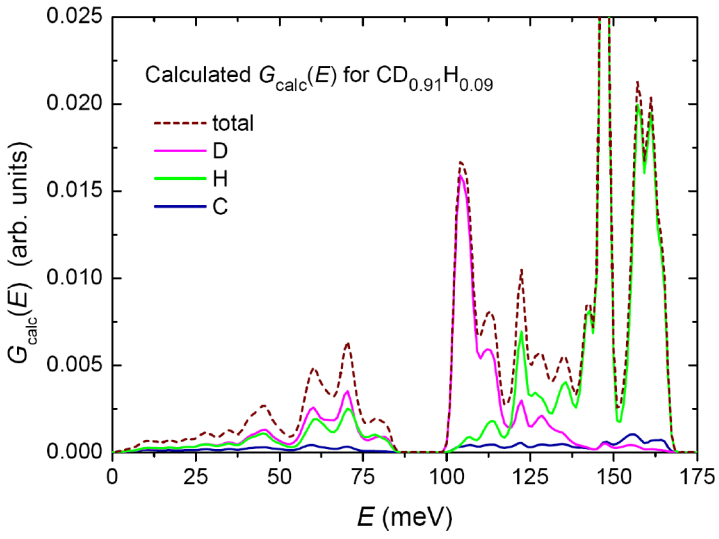

Fig. 8. Calculated total $G_{calc}(E)$ for the graphane II phase of the $CD_{0.91}H_{0.09}$ compound (dashed brown curve) obtained as the sum of partial contributions $G_i(E)$ from neutron scattering by the C, D, and H atoms (solid colored curves). Each calculated spectrum is convoluted with the energy resolution function of the SEQUOIA spectrometer.

The last problem to be discussed in this section is the change in the vibrational energies resulting from the replacement of protium with deuterium in the graphane II compound. The peak of stretching vibrations descends from 351 meV in the hydride to 258 meV in the deuteride (see Fig. 4b). These vibrations of the C-H or C-D groups are approximately perpendicular to the graphane layers and are only slightly perturbed by interactions with other atoms of the layer. Accordingly, the energy of these vibrations is determined by the reduced mass of the group and should decrease by a factor of $\sqrt{m_{CD}^{red} / m_{CH}^{red}} \approx 1.362$ when protium is replaced by deuterium. The experimental ratio 351/258 ≈ 1.360(4) is equal to this value within the experimental error.

If the energy of long-wavelength acoustic vibrations tends to zero, then the C and H atoms in the C-H groups and the C and D atoms in the C-D groups move in phase, so the ratio of their vibrational energies in the hydride and deuteride, respectively, should be $\sqrt{(m_C + m_D)/(m_C + m_H)} \approx 1.038$. In the lower-energy bands of the hydride and deuteride, there are four peaks, which are most clearly visible in the curves $g_{calc}(E)$ in Fig. 6b. As shown in Fig. S4 in Supplementary Material, the experimental E_H/E_D ratio decreases from 1.16(1) for the peak at E_H = 82 meV to 1.05(2) at E_H = 10 meV. Linear extrapolation to E_H = 0 gives E_H/E_D = 1.034(10) in agreement with the theoretical value of 1.038.

3.3. Equation of state V(P) of graphite hydride

A sample of graphite hydride was studied at room temperature by Synchrotron X-ray diffraction in a diamond anvil cell upon a step-wise increase in the H_2 pressure from 0.3 to 53 GPa. Typical diffraction patterns are shown in Fig. 9. The large residual *R*-factors of the profile fitting are mainly due to the overlap of the diffraction lines of the sample with those of the Au chip used as a pressure gauge, and also with the lines of the Re gasket and its hydrogenated inner edge, whose hydrogen content gradually increased with increasing pressure. The lattice parameters of the hydride were determined using only the angular positions of the 002 and 110 lines, which could be satisfactorily determined at all experimental pressures. The obtained pressure dependences of the atomic volume V_a of graphite hydride and its c/a ratio are shown in Fig. 10 with open red circles.

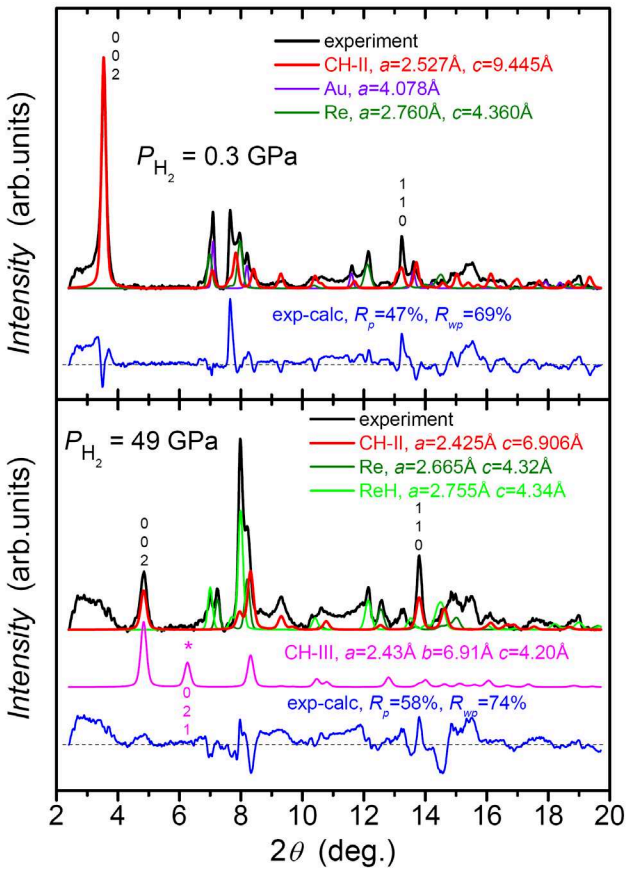

Fig. 9. X-ray diffraction patterns of graphite hydride measured at room temperature and hydrogen pressures of 0.3 GPa (top panel) and 49 GPa (bottom panel) using synchrotron radiation with λ = 0.2914 Å at the P02.2 beamline at PETRA-III (black curves) and results of semi-quantitative profile analysis of these patterns (colored curves).

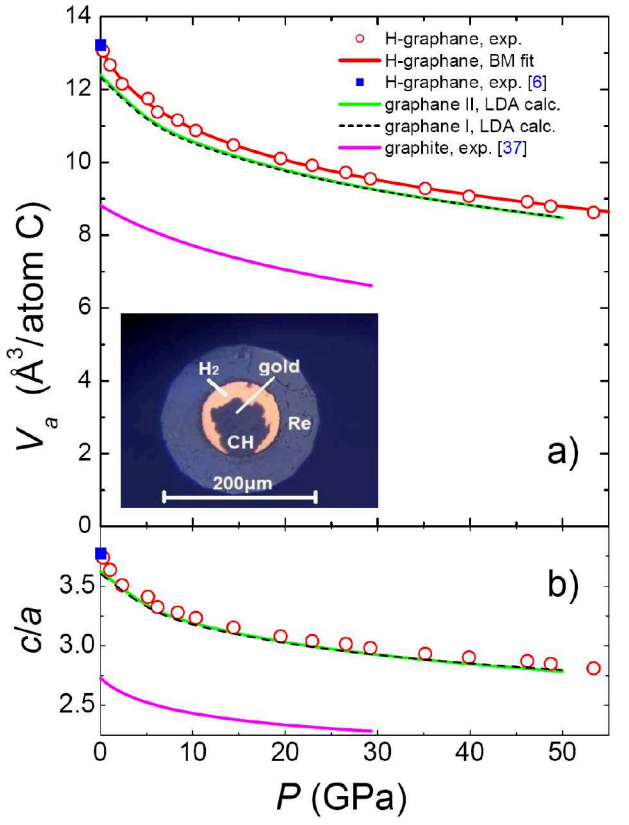

Fig. 10. Experimental pressure dependences of the atomic volume $V_a = (\sqrt{3}/8)a^2c$ (top panel) and c/a ratio (bottom panel) for graphite hydride (open red circles, this paper; solid blue squares, results of Ref [6]) and for graphite (magenta curves, results of Ref. [41]) measured at room temperature. The red curve in the top panel is a fit to the $V_a(P)$ points for graphite hydride using the Birch-Murnaghan equation of state. The solid green curves and dashed black curves represent results of the DFT-LDA calculations for the graphane II and graphane I phases at T = 0 K (the c/a ratio for the graphane I phase in figure (b) is doubled for ease of comparison). The inset in the top panel shows a photo of the sample of graphite hydride at 0.3 GPa.

As seen from Fig. 10, the experimental pressure dependences of V_a and c/a of graphite hydride (open red circles) are in good agreement with the results of previous X-ray diffraction measurements [6] at normal conditions (solid blue squares). The red curve in Fig. 10a shows a fit to the $V_a(P)$ points for graphite hydride using the third-order Birch-Murnaghan equation of state [17,18] determined by three parameters: atomic volume $V_0 = 13.19 \pm 0.03$ Å^3 at $P = 0$; bulk modulus $B_0 = 22.5 \pm 3$ GPa at $P = 0$, and pressure derivative $B_0' = 10.1 \pm 2$ of the bulk modulus. The equation of state with constant values of V_0 and B_0 well approximates the experimental dependence $V_a(P)$, and the value of V_0 agrees with the experimental value of V_a(1 atm) = 13.22(1) Å^3/atom C from Ref. [6]. This is characteristic of hydrides with an invariable H content experiencing no phase transitions.

Our DFT-LDA calculations for the graphane II phase satisfactorily describe the experimental pressure dependences of both V_a and a/c of the graphite hydride (compare the green curves in Figs. 10a and 10b, respectively, with the experimental data). These calculations additionally give a pressure dependence of the distance $d_{C–H}$ between the nearest C and H atoms, which cannot be determined by X-ray diffraction because of the small scattering length of H atoms. Namely, according to the calculations, an increase in pressure from 1 atm to 50 GPa reduces $d_{C–H}$ by 3%, from 1.12 to 1.09 Å, while the distance $c/2$ between the graphane layers decreases by 26%, from 4.547 to 3.360 Å (compare the calculated data in "CH-II_calc.cel" and "CH-II_calc_50GPa.cel" in Supplementary Material).

For comparison, Fig. 10 also shows experimental pressure dependences of V_a and c/a for graphite at room temperature [41]. In contrast to the graphane II phase, these dependences can only be measured at pressures up to about 30 GPa due to the transition of graphite into a post-graphite phase called M-carbon; the transition begins at a pressure of the order of 15 GPa and ends at about 37 GPa [41]. Fitting the experimental $V_a(P)$ dependence for graphite with the third-order Birch-Murnaghan equation of state gave $V_0 = 8.817(11)$ Å^3/atom C and $B_0 = 57.3(8)$ GPa, provided that $B_0' = 4$ [41]. The value of $B_0 = 22.5$ GPa for graphane is predictably smaller due to the greater distance between the carbon layers bound together by weak van der Waals forces.

At pressures up to 53 GPa, our sample of graphite hydride did not react with the surrounding hydrogen and did not transform into the graphane III phase, otherwise we would have seen the diffraction peak 021 of this phase (a calculated diffraction pattern of the graphane III phase at a pressure of 49 GPa is shown in Fig. 9 with a magenta curve; the 021 peak is marked with an asterisk). At the same time, the quality of the X-ray diffraction patterns measured in diamond anvils was insufficient to detect the transition of the graphane II phase to the graphane I phase. The calculated pressure dependences of V and c/a for these phases are very similar (Fig. 10) and cannot help to distinguish the phases either. However, the formation of the graphane I phase at

high pressures is unlikely, since according to the *ab initio* calculations at $T = 0$ K [4], the enthalpy of the graphane II phase is virtually equal to the enthalpy of the graphane I phase at pressures up to 100 GPa and becomes lower at higher pressures, which increases the relative stability of graphane II.

To initiate phase transformations of the graphane II phase at the maximum pressure of 53 GPa, the sample of graphite hydride was laser heated to 1500±500 K with a pulsed Yb-doped fiber IR laser at P02.2 [33]. Subsequent X-ray examination of the sample at room temperature showed no changes in its diffraction pattern. This suggests a possible increase in the thermal stability of the graphane II phase with increasing pressure. Indeed, when a sample of graphite hydride is heated in vacuum at a rate of 20 K/min, it decomposes into graphite and gaseous H_2 in the temperature interval of 830–920 K [6]. When the hydride is heated in molecular hydrogen compressed to 7.5 GPa, it reacts with hydrogen, transforms into methane and/or other light hydrocarbons at 990–1050 K, and therefore disappears as a solid phase [6]. In this paper, the hydride remained intact after heating to ~1500 K at a hydrogen pressure of 53 GPa.

The large *T*-*P* domain of (meta) stability makes the graphane II phase an important member of the carbon-hydrogen system.

3.4. Heat capacity of graphite hydride and deuteride

As one can see from Fig. 11, our calorimetric study of the graphite powder used to synthesize graphite hydride and deuteride showed that its heat capacity agrees with the reference data [42,43] for the bulk graphite. To minimize the effects of a gradual baseline shift, the experimental $C_P(T)$ dependence was composed of segments measured in overlapping temperature intervals with a width of 60–120 K. The dashed orange curve starting at 473 K reflects the initial transient process, which was characteristic of each measurement and continued for about 20 K. The solid colored curves in Fig. 11 show the valid calorimetric results obtained at temperatures above these transient intervals.

Unlike graphite with metallic conductivity, all modifications of one-layer and multilayer graphane are predicted to be dielectrics [4]. The electronic band structure of the graphane II phase calculated by DFT-LDA is shown in Fig. S5 in Supplementary Material. The gap width of about 3.3 eV in the electronic spectrum agrees with the results of similar previous calculations [4]. More advanced calculations using many-body GW approximations, which include electron-electron interactions beyond DFT, give a much larger band gap of 5.4–6.1 eV for one-layer graphane in the chair conformation [44,45]. In any case, the graphite hydride and deuteride studied in this work are undoubtedly dielectrics, and their heat capacity is exclusively of phonon origin.

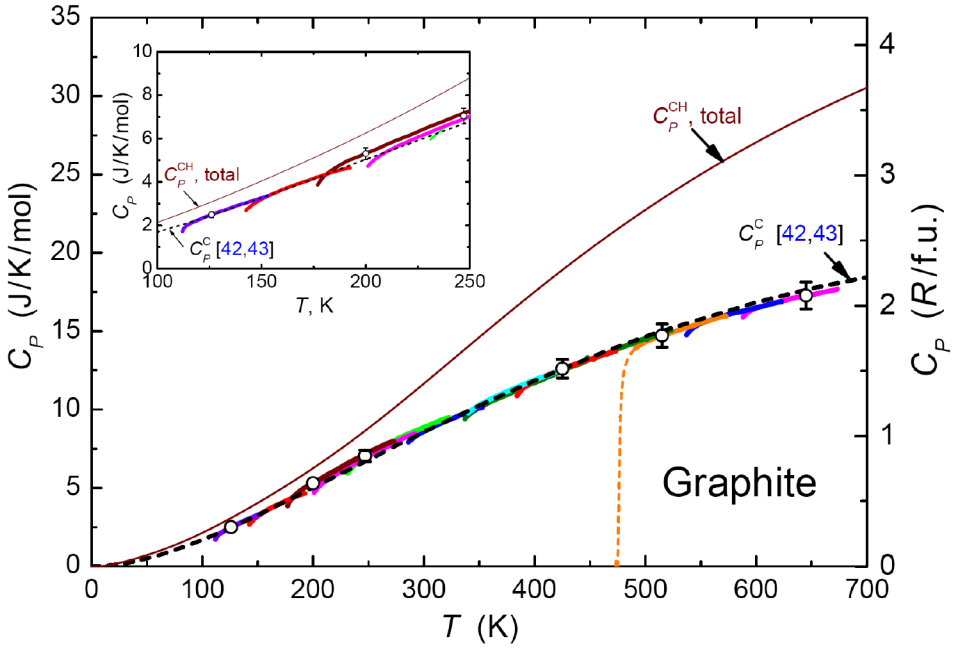

Fig. 11. Experimental temperature dependences of the heat capacity C_P of graphite powder measured in this paper at a heating rate of 20 K/min (segments of thick colored curves) and C_P of bulk graphite reported in Refs. [42,43] (dashed black curve). The thin brown curve labeled "C_P^{CH}, total" shows the heat capacity calculated for the graphane II phase of graphite hydride (this dependence is borrowed from Fig. 12, where it is depicted as a dashed black curve). Some experimental points are shown as open black circles intersected by vertical bars, which indicate the experimental error of 5% of the Perkin-Elmer DSC 7 scanning calorimeter used in the present study. R = 8.314 J/mole/K is the universal gas constant. The inset shows the results for lower temperatures on a larger scale.

The spectra $g_{exp}(T)$ and $g_{calc}(T)$ of the phonon density of states discussed in section 3.1 and 3.2 were used to calculate the heat capacities for the corresponding graphane II phases of graphite hydride and deuteride at temperatures up to 1000 K. The heat capacities $C_V(T)$ at constant volume were calculated as:

$$C_V(T) = \frac{R}{4} \cdot \int \left(\frac{E}{k_B T} \right)^2 g(E) n(E,T) \left[n(E,T) + 1 \right] \mathrm{d}E, \qquad (1)$$

where R = 8.314 J/mole/K is the universal gas constant; k_B = $1.381 \cdot 10^{-23}$ J/K is the Boltzmann constant, and $n(E,T) = \left[\exp\left(E/k_B T\right) - 1 \right]^{-1}$ is the Bose factor. With the phonon spectra normalized to 24 states in total, this equation gives $C_V(T) \xrightarrow{T \to \infty} 6R = 3R \times 2$ per gram-mole of the hydride (CH) or deuteride (CD) in accordance with the Dulong and Petit law. The contributions to the heat capacity from the lower-, middle-, and upper-energy bands were also calculated separately and

shown in the Figures. In addition, the dependences of the heat capacity $C_P(T)$ at constant pressure were calculated from the corresponding dependences of the heat capacity $C_V(T)$ at constant volume by adding a small difference $\Delta C_{PV}^{\mathrm{CH}} = C_P(T) - C_V(T)$ determined for graphite hydride; the details of the determination of $\Delta C_{PV}^{\mathrm{CH}}(T)$ will be discussed in this section later.

The investigated samples of graphite hydride and deuteride contained, respectively, 6 and 5 mol.% of unreacted graphite. The measured calorimetric data for these samples were corrected to represent $C_P(T)$ of pure graphite hydride CH and deuteride CD using the experimental dependence $C_P(T)$ of graphite from Refs. [42,43] (dashed black curve in Fig. 11). The corrections were small and only reached about 1% at the maximum measurement temperature of 673 K.

As seen from Fig. 12, the experimental $C_P(T)$ dependence for graphite hydride is rather well approximated with the "C_P^{CH}, total INS" dependence (orange curve) based on $g_{\mathrm{exp}}(E)$ derived from the INS study and shown by the red curve in Fig. 5a. An equally good fit is provided by the "C_P^{CH}, total" dependence (dashed black curve) resulting from $g_{\mathrm{calc}}(E)$ calculated by DFT-LDA and shown by the red curve in Fig. 6. A considerable deviation of the DFT-LDA dependence from experiment was only observed at the lowest temperatures $T < 150$ K (see inset in Fig. 12). The reason for this deviation remains unclear.

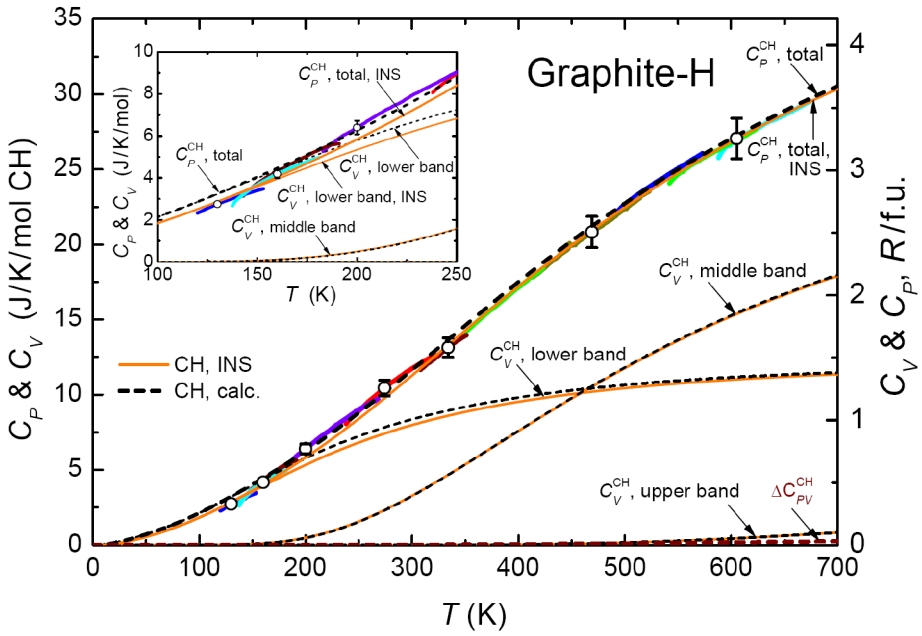

Fig. 12. Temperature dependences of the heat capacity of graphite hydride determined experimentally (thick colored curves) and those calculated from the INS-derived $g_{\mathrm{exp}}(E)$ (thin orange curves). Dashed black curves show the heat capacity of the graphane II phase of graphite hydride resulting from the $g_{\mathrm{calc}}(E)$ calculated by DFT-LDA. The curves labeled "C_P^{CH}, total" and "C_P^{CH}, total INS" are obtained by adding the difference labeled "$\Delta C_{PV}^{\mathrm{CH}}$" to the corresponding calculated dependences of the total $C_V(T)$.

The approximate composition of the graphite deuteride synthesized and studied in this work was $CD_{0.91}H_{0.09}$. In Fig. 13, the experimental heat capacity of this deuteride is compared with the $C_P(T)$ dependences calculated for the graphane II phases of $CD_{0.875}H_{0.125}$ (solid grey curve) and pure CD (dashed black curve); the $g_{calc}(E)$ spectra used to calculate these dependences are shown in Fig. 7. As can be seen from Fig. 13, the two calculated $C_P(T)$ dependences almost coincide with each other and well approximate the experimental dependence over the entire studied temperature interval of 120–673 K. This suggests, in particular, that $C_P(T)$ and $g_{calc}(E)$ calculated by DFT-LDA for the graphane II phase of hydrogen-free graphite deuteride should accurately reproduce the properties of this CD compound.

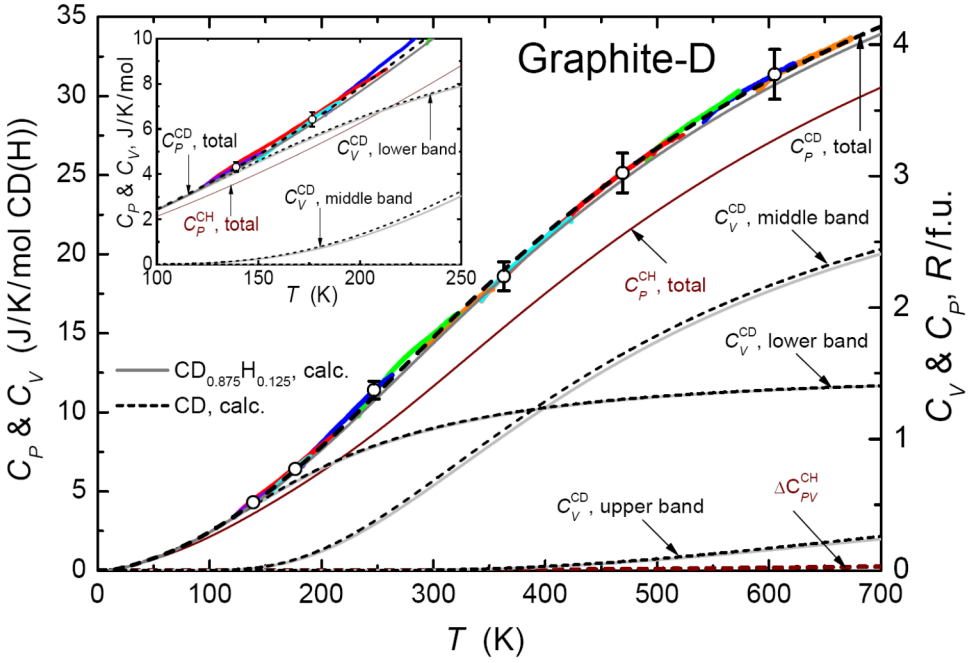

Fig. 13. Temperature dependence of the experimental heat capacity of graphite deuteride with the composition $CD_{0.91}H_{0.09}$ (thick colored curves) and calculated dependences of the heat capacity of the graphane II phases of deuterides CD (dashed black curves) and $CD_{0.875}H_{0.125}$ (solid grey curves). The dependences of the calculated heat capacity at constant pressure are obtained from the corresponding $C_V(T)$ dependences by adding the "ΔC_{PV}^{CH}" difference determined for the graphite hydride.

3.5. Estimation of $C_P(T) - C_V(T)$ for graphite hydride

The $C_V(T)$ dependences calculated using Equation (1) refer to the volume of multilayer graphane at the temperature of determining the phonon spectrum, i.e., $V(0\ \mathrm{K})$ for $g_{calc}(E)$ calculated by DFT-LDA, or $V(5\ \mathrm{K}) \approx V(0\ \mathrm{K})$ for $g_{exp}(E)$ derived from the INS data. The $C_V(T)$ dependence can be converted into $C_P(T)$ required for thermodynamic analysis by adding the correction term

$$\Delta C_{PV} = C_P - C_V = \alpha^2 VT/\beta, \qquad (2)$$

where V is the molar volume; $\alpha = (1/V)(\partial V/\partial T)_P$ is the coefficient of volume expansion, and $\beta = 1/B_0 = -(1/V)(\partial V/\partial P)_T$ is the isothermal compressibility, all of these factors being functions of temperature [46].

To determine $\alpha(T)$ and $V(T)$, a small portion of the hydride sample was studied by X-ray diffraction at ambient pressure and temperatures from 297 to 573 K. The obtained $V_a(T)$ dependence is shown in Fig. 14 by open blue circles.

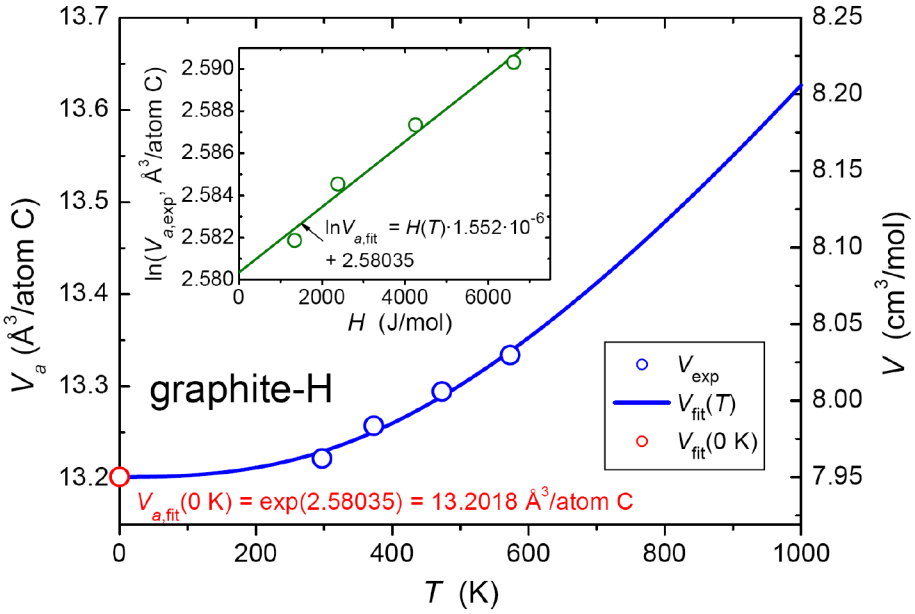

Fig. 14. Experimental temperature dependence of the atomic volume $V_a = (\sqrt{3}/8)a^2c$ of graphite hydride at ambient pressure (open blue circles) approximated by Equation (3) as shown in the inset.

One of the semi-empirical Grüneisen laws says that α is approximately proportional to the heat capacity (see [46]). From $\alpha(T) = A \cdot C_V(T)$ it follows that

$$\ln[V(T)/V(0K)] = A\int_0^T C_V(\tau)\mathrm{d}\tau, \quad (3)$$

where $\int_0^T C_V(\tau)\mathrm{d}\tau$ is actually the enthalpy $H(T)$. Linear approximation of the experimental $\ln[V_{a,\mathrm{exp}}(H)]$ dependence (see inset to Fig. 14) gave us the fitting parameters A = 1.552·10^{-6} mol/J and $V_{a,\mathrm{fit}}$ (0 K) = 13.2018 Å^3/atom C. The resulting $V_{a,\mathrm{fit}}$ (T) dependence extrapolated down to T = 0 K and up to T = 1000 K is shown in Fig. 14 with a blue curve; the $\alpha_{\mathrm{fit}}(T)$ dependence is depicted in Fig. 15 with a red curve.

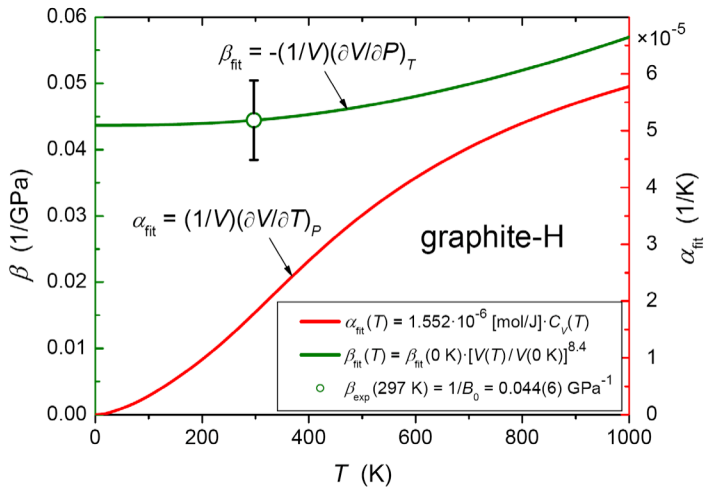

Fig. 15. Temperature dependences of the volume expansion coefficient α_{fit} and isothermal compressibility β_{fit} obtained by fitting the experimental data for graphite hydride using Equations (3) and (4), respectively.

The experimental dependences $a(T)$ and $c(T)$ were also fitted using equations analogous to Equation (3) (see Fig. S6 in Supplementary Material). Such a procedure was earlier demonstrated to give accurate values of lattice parameters extrapolated to 0 K for rather anisotropic hexagonal systems [47] and hydrides AlH_3 [48] and MgH_2 [40]. For the graphite hydride, the extrapolated values of a_{fit}(0 K) = 2.5296 Å and c_{fit}(0 K) =9.5292 Å gave V_a (0 K) = 13.2017 Å^3/atom C, which is very close to $V_{a,\mathrm{fit}}$ (0 K) = 13.2018 Å^3/atom C. This suggests that Equation (3) and its analogs approximate well each of the $V_a(T)$, $a(T)$, and $c(T)$ experimental dependences for graphite hydride at $T \leq 573$ K.

The use of Equation (2) requires knowledge of the $\beta(T)$ dependence as well. This dependence can be obtained from another Grüneisen's semi-empirical relation claiming that $(1/\beta)(\partial\beta/\partial T)_P \approx 8.4\alpha$ (see [49] for discussion and references). Correspondingly,

$$\beta(T) = \beta(0\ \mathrm{K})[V(T)/V(0\ \mathrm{K})]^{8.4}. \quad (4)$$

Using the $V_{fit}(T)$ dependence shown in Fig. 14 and drawing dependence (4) through the experimental point $\beta(297\ K) = 1/B_0 = 0.044(6)\ GPa^{-1}$ gave the fitting parameter $\beta(0\ K) = 0.0437\ GPa^{-1} \approx \beta(297\ K)$. The resulting $\beta_{fit}(T)$ dependence is plotted in Fig. 15 by an olive curve.

Substituting the $\alpha_{fit}(T)$, $V_{fit}(T)$, and $\beta_{fit}(T)$ dependences thus obtained into Equation (2) gave the $\Delta C_{PV}^{CH}(T)$ dependence shown by the dashed brown curves at the bottom of Figs. 12 and 13, and—on a larger scale—in Fig. S7 in Supplementary Material. Due to the high compressibility of the multilayer graphane, the correction $\Delta C_{PV}^{CH}(T)$ is small compared to $C_V(T)$ and only reaches about 0.5 J/K/mol at $T = 1000$ K, which is less than 1.5% of $C_V(1000\ K)$.

4. Concluding remarks

In its compounds carbon forms very strong chemical bonds with hydrogen. Among the stable at ambient conditions hydrocarbons, methane CH_4 has the highest gravimetric hydrogen capacity of 25 wt. % H. Methane can be thermally and thermocatalytically decomposed into carbon and hydrogen without the formation of carbon oxides. A variety of the processes using methane as a clean source of hydrogen is considered in a review paper [50].

Various carbon-based materials including activated carbon, graphite, graphene, graphene oxide, reduced graphene oxide, fullerenes, and carbon nanotubes have been examined as possible hydrogen hosts in H_2 storage systems. For most of these materials, the mechanism of hydrogen storage is H_2 physisorption. Using the materials with a large surface area of 1000 m^2/g or more in combination with cryocooling made it possible to reach H storage capacities exceeding 3 wt.% H. These materials alone do not meet the requirements for the hydrogen system performance. However, they can be modified through either decoration or doping to alter their chemical properties and increase their hydrogen storage capacity, by applying various metal-modified graphene materials [51].

Graphene-based materials have also been considered for use in solid-state hydrogen storage, because of their large specific surface area. However, graphene is additionally capable of forming C-H chemical bonds like other carbon-based materials, which significantly increases its hydrogen storage capacity at ambient temperatures and above. Solid-state hydrides with the C–H chemical bonds and H storage capacities reaching 7.7 wt.% for the stoichiometric composition CH were reported for fullerenes C_{60} and C_{70} [52,53], carbon nanotubes [54], and graphite after its mechanochemical treatment in gaseous hydrogen [19].

Single-layer sheets of graphene have been shown to react with atomic hydrogen and demonstrate reversibility of their hydrogen storage performance [3]. In fact, the formation of

graphane was registered after a 2-hour treatment of graphene in dc plasma ignited in a mixture of 10 % H_2 with argon at a pressure of 10 Pa. The original state of the graphene sample was restored after hydrogen desorption at 723 K in an Ar atmosphere for 24 h. Bulk graphite also belongs to the materials that reversibly absorb and desorb hydrogen: multilayer graphane is formed from graphite and hydrogen at pressures above 2 GPa and temperatures 720–970 K and decomposes back into graphite and molecular hydrogen when heated in vacuum to 770–920 K [6].

The relative stability of various possible phases of multilayer graphane at $T = 0$ K has been carefully examined by first-principles calculations in Ref. [4]. The theoretical studies showed that two phases called graphane I and graphane II and consisting of the layers of 2D-graphane in the chair conformation are almost equally stable at pressures up to 10 GPa, and the graphane III phase built from graphane layers in the boat conformation is the most stable phase at pressures from 10 to 240 GPa. In Ref. [6], multilayer graphane was shown to form from graphite and molecular hydrogen at hydrogen pressures of 2 to 7.5 GPa and elevated temperatures. A semi-quantitative profile analysis of the X-ray diffraction patterns of the synthesized samples showed [6] that one of the two phases predicted to be stable in the studied pressure range, the graphane II phase, provides a satisfactory fit to the measured patterns, whereas the graphane I phase does not.

In this paper, an INS investigation gave the spectrum $g_{exp}(E)$ of the phonon density of states for the multilayer graphane, which proved to be very similar to the $g_{calc}(E)$ spectrum of the graphane II phase predicted by first-principles calculations, including the presence of a gap between the lower- and middle-energy vibrational bands. The gap is characteristic of the phonon spectrum of one-layer graphane in the chair conformation [13]. It remains almost the same in the spectra of the graphane I and graphane II phases consisting of such layers, and is absent in the spectra of other phases of 3D-graphane [4]. The accurate prediction of both the crystal structure and phonon spectrum of multilayer graphane validates the results of the first-principles calculations. Of the three phases (graphane I, II, and III) expected to be stable at pressures below 240 GPa, X-ray diffraction [6] and inelastic neutron scattering (this paper) unequivocally selected the graphane II phase as the one which is preferably formed.

As mentioned in section 1, recent *ab initio* calculations of phase equilibria in the C-H system showed [5] that the graphane I and graphane III phases are not thermodynamically stable at hydrogen pressures up to 400 GPa and temperatures from 500 to 2000 K. Apparently, the graphane II phase studied in this work should also be considered as a metastable phase, which is typical of many hydrocarbons. At the same time, the domain of baric and thermal stability of this phase is extremely large: once formed at a hydrogen pressure of 7.4 GPa and a temperature of 870 K, the graphane II sample did not react with the surrounding hydrogen and did not transform to any other phases without changing the chemical composition even at a pressure as high as 53 GPa and a

temperature exceeding 1000 K (see section 3.3). Accordingly, the graphane II phase is an important part of the vital carbon-hydrogen system and deserves thorough investigations.

To facilitate further experimental and theoretical studies, some results of this paper are presented in numerical format in Supplementary Material. Table S1 presents the phonon densities of states $g_{calc}(E)$ for the graphane II phases of graphite hydride and deuteride calculated by DFT-LDA and slightly corrected to better represent the experimental INS spectra (see section 2.4); the tabulated $g_{calc}(E)$ are shown in Fig. 6. Table S2H and Table S2D present the dependences $C_V(T)$, $\Delta C_{PV}(T)$, and $C_P(T)$ for the graphane II phases of, respectively, graphite hydride and deuteride calculated using $g_{calc}(E)$ from Table S1; these dependences are shown in Figs. 12 and 13 by the dashed curves. Table S3H and Table S3D contain temperature dependences of the standard (referred to P_0 = 1 atm) enthalpy $H^0 = \int_0^T C_P(\tau)\mathrm{d}\tau$, standard entropy $S^0 = \int_0^T [C_P(\tau)/\tau]\mathrm{d}\tau$, and standard Gibbs free energy $G^0 = H^0 - T{\cdot}S^0$ for this hydride and deuteride. Supplementary Material also includes CEL files with the structural parameters of the studied phases of multilayer graphane; the data in the file "CH-II_exp.cel" are taken from Ref. [6] and refer to room temperature, the data in the other CEL files are the results of our DFT-LDA calculations.

CRediT authorship contribution statement

V.A. Yartys: Supervision, Project administration, Validation, Writing – review & editing. **V.E. Antonov:** Conceptualization, Visualization, Writing – original draft. **B.N. Bulychev:** Resources. **V.S. Efimchenko:** Investigation. **V.I. Kulakov:** Investigation. **M.A. Kuzovnikov:** Investigation, Formal analysis, Visualization, Writing – original draft. **R.T. Howie:** Investigation. **H.A. Shuttleworth:** Investigation. **M. Holin:** Investigation. **R. Rae:** Investigation. **M.B. Stone:** Investigation. **B.P. Tarasov:** Resources. **R.I. Usmanov:** Investigation. **A.I. Kolesnikov:** Investigation, Formal analysis, Writing – review & editing.

Declaration of competing interest

Authors hereby declare that there is no conflict of interest for the research work reported in this manuscript.

Acknowledgments

This manuscript has been authored by UT-Battelle, LLC under Contract No. DE-AC05-00OR22725 with the U.S. Department of Energy. The United States Government retains and the publisher, by accepting the article for publication, acknowledges that the United States Government retains a non-exclusive, paid-up, irrevocable, world-wide license to publish or reproduce the published form of this manuscript, or allow others to do so, for United States Government purposes. The Department of Energy will provide public access to these results of federally sponsored research in accordance with the DOE Public Access Plan (http://energy.gov/downloads/doe-public-access-plan). The work was funded by the Russian Science Foundation under project no. 23-22-00361 and by the Horizon 2020 program of the European Union (Grant no. 948895, MetElOne). A portion of the research used resources at the Spallation Neutron Source, a DOE Office of Science User Facility operated by the Oak Ridge National Laboratory. The beam time was allocated to SEQUOIA spectrometer on Proposal No. IPTS-31213.1. We acknowledge DESY (Hamburg, Germany), a member of the Helmholtz Association HGF, for the provision of experimental facilities. Parts of this research were carried out at beamline P02.2 at PETRA-III. Beamtime was allocated for proposal I-20220830.

Appendix A. Supplementary data

Supplementary Material to this article can be found online at https://doi.org/10.1016/j.matchemphys.2024.130232.

References

[1] M.H.F. Sluiter, Y. Kawazoe, Cluster expansion method for adsorption: application to hydrogen chemisorption on graphene, Phys. Rev. B 68 (2003) 085410, https://doi.org/10.1103/PhysRevB.68.085410.

[2] J.O. Sofo, A.S. Chaudhari, G.D. Barber, Graphane: A two-dimensional hydrocarbon, Phys. Rev. B 75 (2007) 153401, https://doi.org/10.1103/PhysRevB.75.153401.

[3] D.C. Elias, R.R. Nair, T.M.G. Mohiuddin, S.V. Morozov, P. Blake, M.P. Halsall, A.C. Ferrari, D.W. Boukhvalov, M.I. Katsnelson, A.K. Geim, K.S. Novoselov, Control of graphene's properties by reversible hydrogenation: evidence for graphane, Science 323 (2009) 610–613, https://doi.org/10.1126/science.1167130.

[4] X.-D. Wen, L. Hand, V. Labet, T. Yang, R. Hoffmann, N.W. Ashcroft, A.R. Oganov, A.O. Lyakhov, Graphane sheets and crystals under pressure, Proc. Nat. Acad. Sci. U. S. A. 108 (2011) 6833–6837, https://doi.org/10.1073/pnas.1103145108.

[5] A.S. Naumova, S.V. Lepeshkin, A.R. Oganov, Hydrocarbons under pressure: Phase diagrams and surprising new compounds in the C−H system, J. Phys. Chem. C 123 (2019) 20497−20501, https://doi.org/10.1021/acs.jpcc.9b01353.

[6] V.E. Antonov, I.O. Bashkin, A.V. Bazhenov, B.M. Bulychev, V.K. Fedotov, T.N. Fursova, A.I. Kolesnikov, V.I. Kulakov, R.V. Lukashev, D.V. Matveev, M.K. Sakharov, Y.M. Shulga, Multilayer graphane synthesized under high hydrogen pressure, Carbon 100 (2016) 465–473 (2016), https://doi.org/10.1016/j.carbon.2015.12.051.

[7] V.I. Artyukhov, L.A. Chernozatonskii, Structure and layer interaction in carbon monofluoride and graphane: A comparative computational study, J. Phys. Chem. A 114 (2010) 5389–5396, https://doi.org/10.1021/jp1003566.

[8] J. Rohrer, P. Hyldgaard, Stacking and band structure of van derWaals bonded graphane multilayers, Phys. Rev. B 83 (2011) 165423, https://doi.org/10.1103/PhysRevB.83.165423.

[9] M.V. Kondrin, N.A. Nikolaev, K.N. Boldyrev, Y.M. Shulga, I.P. Zibrov, V.V. Brazhkin, Bulk graphanes synthesized from benzene and pyridine, CrystEngComm 19 (2017) 958−966, https://doi.org/10.1039/c6ce02327d.

[10] V. Kutcherov, A. Kolesnikov, T. Dyuzheva, V. Brazhkin, Synthesis of hydrocarbons under upper mantle conditions: evidence for theory of abiotic deep petroleum origin, J. Phys. Conf. Ser. 215 (2010) 012103, https://doi.org/10.1088/1742-6596/215/1/012103.

[11] M. Peña-Alvarez, A.V. Brovarone, M.-E. Donnelly, M. Wang, P. Dalladay-Simpson, R. Howie, E. Gregoryanz, In-situ abiogenic methane synthesis from diamond and graphite

under geologically relevant conditions, Nature Commun. 12 (2021) 6387, https://doi.org/10.1038/s41467-021-26664-3.

[12] E. Cadelano, P.L. Palla, S. Giordano, L. Colombo, Elastic properties of hydrogenated graphene, Phys. Rev. B 82 (2010) 235414, https://doi.org/10.1103/PhysRevB.82.235414.

[13] G. Savini, A.C. Ferrari, F. Giustino, First-principles prediction of doped graphane as a high-temperature electron-phonon superconductor, Phys. Rev. Lett. 105 (2010) 037002, https://doi.org/10.1103/PhysRevLett.105.037002.

[14] H. Peelaers, A.D. Hernández-Nieves, O. Leenaerts, B. Partoens, F.M. Peeters, Vibrational properties of graphene fluoride and graphane, Appl. Phys. Lett. 98 (2011) 051914, https://doi.org/10.1063/1.3551712.

[15] M.S. Somayazulu, L.W. Finger, R.J. Hemley, H.K. Mao, High-pressure compounds in methane-hydrogen mixtures, Science 271 (1996) 1400−1402, https://doi.org/10.1126/science.271.5254.1400

[16] U. Ranieri, L.J. Conway, M.-El. Donnelly, H. Hu, M. Wang, P. Dalladay-Simpson, M. Peña-Alvarez, E. Gregoryanz, A. Hermann, R.T. Howie, Formation and stability of dense methane-hydrogen compounds, Phys. Rev. Lett. 128 (2022) 215702, https://doi.org/10.1103/PhysRevLett.128.215702.

[17] F.D. Murnaghan, The compressibility of media under extreme pressures, Proc. Nat. Acad. Sci. U. S. A. 30 (1944) 244–247, https://doi.org/10.1073/pnas.30.9.244.

[18] F. Birch, Finite elastic strain of cubic crystals, Phys. Rev. 71 (1947) 809–824, https://doi.org/10.1103/PhysRev.71.809.

[19] S. Orimo, G. Majer, T. Fukunaga, A. Züttel, L. Schlapbach, H. Fujii, Hydrogen in the mechanically prepared nanostructured graphite, Appl. Phys. Lett. 75 (1999) 3093–3095, https://doi.org/10.1063/1.125241.

[20] V.E. Antonov, B.M. Bulychev, V.K. Fedotov, D.I. Kapustin, V.I. Kulakov, I.A. Sholin, NH_3BH_3 as an internal hydrogen source for high pressure experiments, Int. J. Hydrogen Energy 42 (2017) 22454–22459, https://doi.org/10.1016/j.ijhydene.2017.03.121.

[21] L.G. Khvostantsev, V.N. Slesarev, V.V. Brazhkin, Toroid type high-pressure device: history and prospects, High Pressure Res. 24 (2004) 371–383, https://doi.org/10.1080/08957950412331298761.

[22] G.E. Granroth, A.I. Kolesnikov, T.E. Sherline, J.P. Clancy, K.A. Ross, J.P.C. Ruff, B.D. Gaulin, S.E. Nagler, SEQUOIA: A newly operating chopper spectrometer at the SNS, J. Physics: Conf. Series 251 (2010) 012058, https://doi.org/10.1088/1742-6596/251/1/012058.

[23] A.I. Kolesnikov, I. Natkaniec, V.E. Antonov, I.T. Belash, V.K. Fedotov, J. Krawczyk, J. Mayer, E.G. Ponyatovsky, Neutron spectroscopy of $MnH_{0.86}$, $NiH_{1.05}$, $PdH_{0.99}$ and harmonic behaviour of their optical phonons, Physica B 174 (1991) 257–261, https://doi.org/10.1016/0921-4526(91)90616-M.

[24] V.E. Antonov, I.T. Belash, A.I. Kolesnikov, J. Maier, I. Natkaniec, E.G. Ponyatovskii, V.K. Fedotov, Neutron-scattering study of the vibrational-spectrum of manganese hydride, Fizika Tverdogo Tela 33 (1991) 152–157, WOS:A1991FZ03900028 (in Russian) [Engl. transl.: Sov. Phys. Solid State 33 (1991) 87–90].

[25] V.S. Oskotskii, Measurement of phonon distribution function in polycrystalline materials using coherent scattering of slow neutrons into a solid angle, Fizika Tverdogo Tela (Leningrad) 9 (1967) 550−552 (in Russian) [Engl. transl.: Sov. Phys. Solid State 9 (1967) 420−422].

[26] S.J. Clark, M.D. Segall, C.J. Pickard, P.J. Hasnip, M.I.J. Probert, K.Refson, M.C. Payne, First principles methods using CASTEP, Z. Kristallogr. 220 (2005) 567–570, https://doi.org/10.1524/zkri.220.5.567.65075.

[27] D.M. Ceperley, B.J. Alder, Ground state of the electron gas by a stochastic method, Phys. Rev. Lett. 45 (1980) 566–569, https://doi.org/10.1103/PhysRevLett.45.566.

[28] J.P. Perdew, A. Zunger, Self-interaction correction to density-functional approximations for many-electron systems, Phys. Rev. B 23 (1981) 5048–5079, https://doi.org/10.1103/PhysRevB.23.5048.

[29] N. Ooi, A. Rairkar, J.B. Adams, Density functional study of graphite bulk and surface properties, Carbon 44 (2006) 231–242, https://doi.org/10.1016/j.carbon.2005.07.036.

[30] K. Refson, P.R. Tulip, S.J. Clark, Variational density-functional perturbation theory for dielectrics and lattice dynamics, Phys. Rev. B 73 (2006) 155114, https://doi.org/10.1103/PhysRevB.73.155114.

[31] H.J. Monkhorst, J.D. Pack, Special points for Brillouin-zone integrations, Phys. Rev. B 13 (1976) 5188–5192, https://doi.org/10.1103/PhysRevB.13.5188.

[32] S.M. Dorfman, V.B. Prakapenka, Y. Meng, T.S. Duffy, Intercomparison of pressure standards (Au, Pt, Mo, MgO, NaCl and Ne) to 2.5 Mbar, J. Geophys. Res. 117 (2012) B08210, https://doi.org/10.1029/2012JB009292.

[33] H.-P. Liermann, Z. Konôpková, W. Morgenroth, K. Glazyrin, J. Bednarcik, E. E. McBride, S. Petitgirard, J.T. Delitz, M. Wendt, Y. Bican, A. Ehnes, I. Schwark, A. Rothkirch, M. Tischer, J. Heuer, H. Schulte-Schrepping, T. Kracht, H. Franz, The extreme conditions beamline P02.2 and the extreme conditions science infrastructure at PETRA III, J. Synchrotron Radiat. 22 (2015) 908−924, https://doi.org/10.1107/S1600577515005937.

[34] C. Prescher, V.B. Prakapenka, DIOPTAS: a program for reduction of two-dimensional X-ray diffraction data and data exploration, High Pressure Res. 35 (2015) 223−230, https://doi.org/10.1080/08957959.2015.1059835.

[35] W. Kraus, G. Nolze, POWDER CELL - a program for the representation and manipulation of crystal structures and calculation of the resulting X-ray powder patterns, J. Appl. Cryst. 29 (1996) 301–303, https://doi.org/10.1107/S0021889895014920.

[36] J.W. Arblaster, Crystallographic properties of platinum, Platinum Metals Rev. 50 (2006) 118–119, https://doi.org/10.1595/147106706X129088.

[37] V. Petricek, M. Dusek, L. Palatinus, Crystallographic computing system JANA2006: General features, Z. Kristallogr. 229 (2014) 345–352, https://doi.org/10.1515/zkri-2014-1737.

[38] Neutron scattering lengths and cross sections, https://www.ncnr.nist.gov/resources/n-lengths/.

[39] A.I. Kolesnikov, V.E. Antonov, Y.E. Markushkin, I. Natkaniec, M.K. Sakharov, Lattice dynamics of AlH_3 and AlD_3 by inelastic neutron scattering: High-energy band of optical bond-stretching vibrations, Phys. Rev. B 76 (2007) 064302, https://doi.org/10.1103/PhysRevB.76.064302.

[40] A.I. Kolesnikov, V.E. Antonov, V.S. Efimchenko, G. Granroth, S.N. Klyamkin, A.V. Levchenko, M.K. Sakharov, Y. Ren, Neutron spectroscopy of magnesium dihydride, J. Alloys Compounds 509S (2011) S599–S603, https://doi.org/10.1016/j.jallcom.2010.10.156.

[41] Y. Wang, J.E. Panzik, B. Kiefer, K.K.M. Lee, Crystal structure of graphite under room-temperature compression and decompression, Sci. Rep. 2 (2012) 520, https://doi.org/10.1038/srep00520.

[42] W. DeSorbo, W.W. Tyler, The specific heat of graphite from 13° to 300°K, J. Chem. Phys. 21 (1953) 1660–1663, https://doi.org/10.1063/1.1698640.

[43] A.T.D. Butland, R.J. Maddison, The specific heat of graphite: An evaluation of measurements, J. Nucl. Mater. 49 (1973/74) 45–56, https://doi.org/10.1016/0022-3115(73)90060-3.

[44] S. Lebègue, M. Klintenberg, O. Eriksson, M.I. Katsnelson, Accurate electronic band gap of pure and functionalized graphane from GW calculations, Phys. Rev. B 79 (2009) 245117, https://doi.org/10.1103/PhysRevB.79.245117.

[45] F. Karlický, M. Otyepka, Band gaps and optical spectra of chlorographene, fluorographene and graphane from G_0W_0, GW_0 and GW calculations on top of PBE and HSE06 orbitals, J. Chem. Theory Comput. 9 (2013) 4155–4164, https://doi.org/10.1021/ct400476r.

[46] L.D. Landau, E.M. Lifshitz, Statistical Physics, Part 1, third ed., Pergamon, Oxford, 1980.

[47] F. Sayetat, P. Fertey, M. Kessler, An easy method for the determination of Debye temperature from thermal expansion analyses, J. Appl. Crystrallogr. 31 (1998) 121–127, https://doi.org/10.1107/S0021889897006936.

[48] V.E. Antonov, A.I. Kolesnikov, Yu.E. Markushkin, A.V. Palnichenko, Y. Ren, M.K. Sakharov, Heat capacity of α-AlH_3 and α-AlD_3 at temperatures up to 1000 K, J. Phys.: Condens. Matter 20 (2008) 275204, http://dx.doi.org/10.1088/0953-8984/20/27/275204.

[49] R. Fürth, The stability of crystal lattices. V. Experimental evidence on recent theories of the equation of state and the melting of solids, Proc. Camb. Phil. Soc. 37 (1941) 34–54, https://doi.org/10.1017/S0305004100021514.

[50] H.F. Abbas, W.M.A. Wan Daud, Hydrogen production by methane decomposition: A review, Int. J. Hydrogen Energy 35 (2010) 1160–1190, https://doi.org./10.1016/j.ijhydene.2009.11.036.

[51] L. Sotsky, A. Castillo, H. Ramos, E. Mitchko, J. Heuvel-Horwitz, B. Bick, D. Mahajan, S.S. Wong, Hydrogen storage properties of metal-modified graphene materials, Energies 17 (2024) 3944, https://doi.org/10.3390/en17163944.

[52] B.P. Tarasov, V.N. Fokin, A.P. Moravsky, Yu.M. Shul'ga, V.A. Yartys, Hydrogenation of fullerenes C_{60} and C_{70} in the presence of hydride-forming metals and intermetallic compounds, J. Alloys Compounds 253–254 (1997) 25–28, https://doi.org/10.1016/S0925-8388(96)03073-3.

[53] V.E. Antonov, A.V. Bazhenov, I.O. Bashkin, L.V. Zorina, A.I. Kolesnikov, S.S. Khasanov, V.K. Fedotov, T.N. Fursova, High-pressure hydrofullerites, J. Surface Investigation 14 (2020) 995−1003, https://doi.org/10.1134/S1027451020050237.

[54] I.O. Bashkin, V.E. Antonov, A.V. Bazhenov, I.K. Bdikin, D.N. Borisenko, E.P. Krinichnaya, A.P. Moravsky, A.I. Harkunov, Yu.M .Shul'ga, Yu.A. Ossipyan, E.G. Ponyatovsky, Thermally stable hydrogen compounds obtained under high pressure on the basis of carbon nanotubes and nanofibers, JETP Lett. 79 (2004) 226–230, https://doi.org/10.1134/1.1753421.